Australasian asphaltite strandings: their origin reviewed in light of the effects of weathering and biodegradation on their biomarker and isotopic profiles

P.A Hall[1,4], D.M. McKirdy[1], K. Grice[2] & D. Edwards[3]

1. Organic Geochemistry in Basin Analysis Group, Centre for Tectonics, Resources and Exploration (TRaX), School of Earth and Environmental Sciences, University of Adelaide, SA 5005, Australia

E-mail: tony.hall@adelaide.edu.au

2. Western Australia Organic and Isotope Geochemistry Centre, The Institute for Geoscience Research, Department of Chemistry, Curtin University of Technology, GPO Box U1987 Perth, WA 6845, Australia

3. Geoscience Australia, GPO Box 378, Canberra, ACT 2601, Australia

4. Current address: Sprigg Geobiology Centre, School of Earth and Environmental Sciences, University of Adelaide, SA 5005, Australia

Abstract

Asphaltites, long known to strand along the coastline of southern Australia and as distantly as New Zealand and Macquarie Island, are widely regarded as artefacts of submarine oil seepage. Their remarkably uniform composition suggests a common source: marine shale containing sulfur-rich Type II kerogen, probably deposited during an Early Cretaceous oceanic anoxic event (OAE). Suitable hydrocarbon kitchens may exist in the offshore Bight and Otway basins. The physical character of the asphaltites, including laminations and flow structures, and their degree of alteration, which is not the result of biodegradation or extensive water washing, suggest an origin from subsurface tar mats subsequently exposed by the incision of submarine canyons, with the possible formation of asphaltic volcanoes. API gravities of 4–18° impart quasi-neutral buoyancy, implying many asphaltites were submerged drifters prior to stranding, their degree of weathering reflecting, at least in part, the residence

time in the marine environment. For any individual asphaltite specimen, this will depend on the proximity of the seafloor seep to the stranding site, an important consideration when attempting to locate their point of origin.

This study investigates the hydrocarbon biomarker signatures and *n*-alkane $\delta^{13}C$ profiles of asphaltite specimens from stranding sites on the Eyre Peninsula (n = 2), Kangaroo Island (n = 4) and the Limestone Coast (n = 3), South Australia, and the south island of New Zealand (n = 2). Sub-samples of the interior and weathered surface of each specimen were analysed. No distinction could be made between strandings based on their source-dependent molecular and isotopic signatures, confirming their common origin. Comparison of the interior and exterior sub-samples revealed subtle although consistent differences. Given their degree of degradation and isotopic variance, these Australasian asphaltites seem to be products of low intensity seeps in the Ceduna Sub-basin of the Bight Basin and/or Morum Sub-basin of the Otway Basin.

Keywords

Australasian asphaltites, weathering, oil seeps, tar mats, biomarkers, carbon isotopes, Otway Basin, Bight Basin

1. Introduction

Reports of bitumen strandings on the coastlines of South Australia, Victoria, Tasmania and Western Australia date from the early 19th Century (Sprigg and Woolley, 1963; Currie et al., 1992; Volkman et al., 1992; McKirdy et al., 1994; Padley, 1995; Edwards et al., 1998 and references therein). The locations of these strandings along Australia's southern margin (Fig. 1), and their greater frequency in southeastern South Australia, western Victoria and southern Tasmania, fuelled early petroleum exploration in the region on the assumption that they were sourced from local submarine seepages (Sprigg, 1986; Volkman et al., 1992; McKirdy et al., 1994). Accounts describe a variety of oily substances that can be assigned to three categories,

each with a different origin: oils (crude and refined), waxy bitumens and asphaltites (McKirdy et al., 1986, 1994; Edwards et al., 1998). While the early reports were of 'asphaltum' strandings (now known as asphaltites), waxy bitumens have become more prevalent since the 1960s (Padley, 1995).

The oils, which typically strand as liquid droplets, are likely anthropogenic inputs arising from local maritime traffic (Padley et al., 1993; Padley, 1995). The waxy bitumens have been assigned to several genetic families, distinguished by subtle but systematic differences in their sulfur content, biomarker and stable isotopic signatures (McKirdy, 1984a,b; McKirdy et al., 1986a, 1994; Padley, 1995). Three of these bitumen families contain biomarkers attributable to tropical angiosperms (dipterocarpaceae) and freshwater algae (notably dinoflagellates and race B of the green alga *Botryococcus braunii*). That oils of the same Cenozoic lacustrine source affinity occur in Sumatra suggests that the waxy bitumens originated in Indonesia, an interpretation supported by strandings of similar material along the northern (Summons et al., 1992, 1993) and western (Currie et al., 1992) margins of Australia, with long-distance surface transportation on the Southern Equatorial and Leeuwin currents accounting for their widespread dispersal (McKirdy and Horvath, 1976; McGowran et al., 1997; Edwards et al., 1998).

The focus of the present study is the asphaltites (i.e. the Family 4 coastal bitumens of McKirdy 1984a, b; McKirdy et al., 1986a, 1994). Geochemically quite distinct from the waxy bitumens, these are heavy, sulfur-rich, aromatic-asphaltic crudes (4–18° API; ~4% S; 57–84% asphaltenes) that commonly strand as large, jet-black, ovoid lumps (up to 670 mm across and 7 kg in weight) at the high water mark on medium to high energy, gently sloping sandy beaches (McKirdy et al., 1994; Padley, 1995). Unlike the waxy bitumens, which have positive buoyancy, the Australasian asphaltites are on average slightly denser than seawater and therefore are likely to have resided within the water column prior to stranding. The fresh

strandings have a strong petroliferous odour (Sprigg and Woolley, 1963; Volkman et al., 1992; Padley, 1995; Edwards et al., 1998). Their upper surface is characteristically traversed by shrinkage cracks and, although the interior is pliable when fresh, they become brittle upon storage and exhibit a conchoidal fracture pattern (Fig. 2). Their stable isotopic and molecular compositions (McKirdy et al., 1986, 1994; Currie et al., 1992; Volkman et al., 1992; Dowling et al., 1995; Padley, 1995; Edwards et al., 1998), including their enrichment in metallo-porphyrins (Boreham et al., 2001; Totterdell et al., 2008), make them unique among Australasian crude oils. Moreover, historic (>100 years ago) and more recent strandings at sites in Western Australia, South Australia, Victoria and Tasmania and even as far afield as New Zealand and Macquarie Island (Fig. 1) are of remarkably similar composition, suggesting that they all originated from the same offshore petroleum system (Padley, 1995; Edwards et al., 1998).

The previously established source and age-specific biomarkers of these asphaltites indicate an origin from Cretaceous marine shale deposited under anoxic/sulfidic conditions, probably during an oceanic anoxic event (OAE: McKirdy et al., 1994; Edwards et al., 1998; Boreham et al., 2001). In the Northern Hemisphere the Tethyan and Atlantic oceans are renowned for their extensive organic-rich muds deposited during mid-Cretaceous OAEs (Pancost et al., 2004; Jenkyns, 2010 and references therein). At this time in the Southern Hemisphere, the Indian Ocean and contiguous Toolebuc and Blue Whale seaways likewise were sites of restricted circulation (Fig. 3). Accordingly, euxinic marine sediments have been identified in several of the corresponding Australian depocentres, possibly recording the Cenomanian–Turonian OAE2 (Bonarelli Event) and shorter-lived late Albian oceanic anoxic subevent OAE 1d (Breistroffer Event) (Edwards et al., 1999; Boreham et al., 2001; Struckmeyer et al., 2001; Boreham, 2008; Totterdell et al., 2008).

Boult et al. (2005) proposed seafloor seepage of tar as the likely source for the southern Australian asphaltites whereas Logan et al. (2010), expanding upon one of the hypotheses of Edwards et al. (1998), favoured the idea that they were the end result of oil slick mousse stabilising at the ocean surface prior to stranding.

While the origin of the Australasian asphaltites has long been the subject of debate, as yet no effective *marine* petroleum system has been proven to occur in any basin located along Australia's southern margin. Moreover, using the GeoMark™ database, the asphaltites cannot be matched with any oil produced elsewhere in Australia, or globally (Summons et al., 2001). Since the seepage locations of these enigmatic hydrocarbons remain in question, we have adopted a novel approach to the analysis of individual asphaltite specimens that might yield further clues to their point(s) of origin.

In this study we investigate a suite of asphaltites from four widely separated stranding locales: Limestone Coast (n = 3), Kangaroo Island (n = 4) and Eyre Peninsula (n = 2), all in South Australia, and the south island of New Zealand (n = 2) (Fig.1). Sub-samples taken from the external weathered surface and 'fresh' interior of each asphaltite specimen were analysed by gas chromatography-mass spectrometry (GC-MS) and compound-specific isotope analysis (CSIA) with a view to determining their degree of weathering. Since the latter is largely a function of residence time in the ocean, it has the potential to better constrain the location(s) of the parent seafloor seepage.

2. Materials and methods

2.1 Sample suite

The asphaltite samples analysed in this study are listed in Table 1. Those from Kangaroo Island and the Limestone Coast of South Australia were collected during two surveys of coastal bitumen strandings: Department of Mines and Energy Coastal Bitumen Survey, 1983 and a bimonthly survey from 1990 to 1991 (Padley, 1995). The more recent strandings from the Eyre Peninsula, South Australia and Invercargill, New Zealand were collected by Martin Hand and Christine Lawley (University of Adelaide) and Dallas Bradley (Environment Southland, New Zealand). Subsequent to their collection (or acquisition), and prior to their analysis, the samples were stored under darkness in the crypt of the Mawson Laboratories, University of Adelaide.

2.2 Isolation of saturated and aromatic hydrocarbons

A portion (150 mg) of surface scrapings and the interior of each asphaltite sample was dissolved in a minimum amount of dichloromethane and the asphaltenes precipitated by adding an excess (20 ml) of petroleum ether. Activated copper turnings were then introduced to the solvent flask to remove any associated elemental sulphur. After filtration through glass wool, the asphaltene-free supernatant was rotary evaporated to ~5 ml volume and separated into saturated hydrocarbons, aromatic hydrocarbons and polar compounds by conventional open column chromatography on activated silica gel, eluting respectively with petroleum ether, petroleum ether and dichloromethane (40:60), and dichloromethane and methanol (35:65). After removal of the solvent by rotary evaporation, each of the fractions was accurately weighed. The saturated and aromatic hydrocarbon fractions were then redissolved in hexane and stored below –18°C ready for further analysis.

Following their analysis by GC-MS the saturated hydrocarbon fractions were separated into *n*-alkanes and higher molecular weight branched/cyclic alkanes (naphthenes) by urea

adduction (following a procedure modified from Wakeham and Pease, 1992). The samples were evaporated under nitrogen, and then aliquots of urea, acetone and hexane were added sequentially. Non-adducts were separated by rinsing the urea crystals with hexane. Adducted *n*-alkanes were partitioned into hexane after addition of methanol/H_2O (50:50) to dissolve the urea crystals. The separation procedure was repeated three times to ensure recovery of a pure adduct.

2.3 GC-MS

Analyses were undertaken utilising a Hewlett Packard 6890/5973 gas chromatograph-mass spectrometer (GC-MS) system at the University of Adelaide. Full scan data on the saturated hydrocarbon fractions were acquired over the range 45–500 Da at ~3 scans sec^{-1}. The GC was fitted with a HP5-MS capillary column (30 m length, 0.25 mm inside diameter, i.d., and 0.25 µm coating) and helium was used as the carrier gas at a constant flow rate of 1 ml min^{-1}. A 1 µl-aliquot of sample was injected with a split ratio of 50:1 and an injector temperature of 300ºC. The oven temperature was programmed as follows: 50ºC for 1 min, 50–310ºC at 8ºC min^{-1} and 310ºC for 15 min. Full scan data on the aromatic fractions were acquired over the range 50–500 Da at ~3 scans sec^{-1} using a longer DB5-MS column (60 m length, 0.25 mm i.d. and 0.25 µm coating) with the same carrier gas, flow rate, injector temperature and sample volume as for the saturated hydrocarbon fractions. The sample was injected in pulsed-splitless mode; and the temperature program was 60ºC for 1 min, 60–180ºC at 10ºC min^{-1}, 180–310ºC at 4ºC min^{-1} and 310ºC for 14.5 min. Ten repeat analyses of a calibration standard showed a relative standard deviation (%RSD = [standard deviation / average] x 100) of 2.12% in split mode and 0.75% in pulsed splitless mode.

Selected ion monitoring (SIM) of the saturated hydrocarbon fractions was undertaken using the same column and chromatographic conditions as for full scan analysis of the aromatic hydrocarbon fractions, except for a slightly different temperature program, viz. 50ºC for 1

min, 50–150ºC at 10ºC min^{-1}, 150–310ºC at 2.5ºC min^{-1} and 310ºC for 15 min. Data were acquired for masses 123, 177, 191, 205, 217, 218, 231, 253 and 259 at a dwell time of 20 ms. Individual analytes including biomarkers were identified on the basis of their retention times or mass spectra (Peters and Moldowan, 1993; Peters et al., 2005).

2.4 GC–irMS

Compound-specific isotope analysis (CSIA) of the stable carbon isotopes (^{13}C /^{12}C) targeted the most abundant compounds in the urea adduct and non-adduct sub-fractions of the aliphatic hydrocarbon fraction. A HP6890 gas chromatograph (GC) equipped with a HP6890 autosampler was used in tandem with a Micromass isotope ratio mass spectrometer (*ir*MS) for the isotopic measurements. The operating conditions were those detailed by Dawson et al. (2007). A 60 m x 0.25 mm i.d. x 0.25 μm phase thickness DB-1 capillary column was used. In brief, the GC oven was programmed from 50 to 310°C at 3°C min^{-1}, with initial and final hold times of 1 and 20 min, respectively. The carrier gas was He at a flow rate of 1 ml min^{-1}. The $\delta^{13}C$ data were obtained by integrating the ion currents for masses 44, 45 and 46 from the CO_2 formed by oxidation of each chromatographically separated component, after passing through a quartz furnace packed with copper oxide pellets and maintained at 850°C. Monitoring the accuracy and precision of the $\delta^{13}C$ measurements was achieved by analysing a mixture of reference compounds (viz. the $C_{14,}$ $C_{17,}$ C_{19} and C_{25} *n*-alkanes) with known $\delta^{13}C$ values, determined as described by Dawson et al. (2007). Each sample was analysed two or three times and the average $\delta^{13}C$ values and standard deviation reported in per mil (‰) relative to a CO_2 reference gas calibrated to the Vienna Peedee Belemnite (VPDB). The analytical precision was ±0.4‰ or better,

3. Results and discussion

3.1 Oil-oil correlation

For the purposes of oil-oil correlation, the compositions of the inner 'fresh' portion of each asphaltite specimen were compared in order to minimise possible weathering influences. The suite of selected bulk and biomarker ratios employed in the correlation are summarized in Table 2, with representative chromatograms from the GC–MS analyses shown in Figs. 8 and 9. The $\delta^{13}C$ values of individual n-alkanes, another powerful correlation tool, are summarized in Table 4 and plotted against their respective carbon numbers in Fig. 10.

In terms of their bulk composition, the asphaltites display some variation in the relative proportions of saturated hydrocarbons, aromatic hydrocarbons, polar compounds and asphaltenes, although the relative standard deviation (RSD) is <15%. The saturated hydrocarbon fractions (TIC, Fig. 8A) have a unimodal n-alkane distribution ranging from C_{13} to >C_{39}, with a maximum between C_{16} and C_{18} and little odd over even preference (CPI = 1.02–1.04). Among the acyclic alkanes, the ratio of pristane (Pr) to phytane (Ph) is uniform at 1.06–1.14 with a RSD of 3%, whilst Pr/n-C_{17} and Ph/n-C_{18} both have a RSD of 8% (range 0.47–0.58 and 0.40–0.52, respectively).

The terpane distributions of the asphaltites are similar (*m/z* 191, Fig. 8B), with the majority of the measured parameters exhibiting deviations of <10%. Likewise, the sterane distributions correlate well (*m/z* 217, Fig. 8C) with RSDs for C_{27}:C_{28}:C_{29} ααα 20R and C_{27}:C_{28}:C_{29} αββ 20(R+S) being <5% and <3%, respectively. The tricyclic/pentacyclic terpane ratio is more variable (RSD 15%), probably due to the lower relative abundances of tricyclic homologues, whilst the sterane/terpane values are within 9% RSD. $\delta^{13}C$ values for the C_{15}–C_{30} n-alkanes lie between –33.3 and –36.7‰ and display a reasonable degree of correlation (Fig. 10A). The average variation is ±1.1‰ per homologue, with a maximum of ±1.4‰ for n-C_{19}.

The triaromatic steroid distributions (*m/z* 231, Fig. 8D) yield C_{26}:C_{27}:C_{28}:C_{29} values within 6% RSD for all samples. Naphthalene and the methylnaphthalenes are present only at trace levels, with concentrations progressively rising through the dimethyl, trimethyl and

tetramethylnaphthalene isomers. This is partly attributable to evaporation during sample preparation for GC-MS analysis (e.g. Ahmed and George, 2004) and possibly also to evaporation during sample storage prior to analysis. The distributions of identifiable polyaromatic hydrocarbons are alike in all samples, although the dibenzothiophenes show much greater variation with RSDs for DBT/MDBT and DBT/C3DBT of 32% and 51%, respectively.

The compositional uniformity of the sample suite, evident across such a broad spectrum of parameters, is a clear indication that these asphaltites belong to the same oil family, notwithstanding their disparate stranding localities. Moreover, their bulk compositions and biomarker distributions are remarkably similar to those previously reported for other stranded southern Australian asphaltites (Currie et al., 1992; Volkman et al., 1992; McKirdy et al., 1994; Padley, 1995; Edwards et al., 1998; Boreham et al., 2001).

The saturated hydrocarbons of unweathered Australasian asphaltites (Volkman et al., 1992; Padley, 1995; Edwards et al., 1998) share many of the compositional characteristics of a typical marine crude oil. Their n-alkane profile is unimodal (range C_{10}–C_{35+}, maximum at C_{15}/C_{17}) and devoid of odd or even carbon-number predominance. The ratio of pristane to phytane is low (1.1–1.3), indicative of the anoxic depositional environment of the source rock (Powell and McKirdy, 1973). Their terpane distribution exhibits a dominance of C_{30} $\alpha\beta$-hopane, a Ts/Tm ratio <1 (Ts = C_{27} 18α(H)-22,29,30-trisnorneohopane; Tm = C_{27} 17α(H)-22,29,30-trisnorhopane), the presence of both 29,30- and 28,30-bisnorhopanes, and a lack of both 25-norhopanes and land-plant biomarkers (e.g. oleanane and bicadinanes). However, unlike other oils of marine source affinity, their triterpanes do not include 2α- and 3β-methylhopanes. Their regular steranes (C_{27}≥C_{29}>C_{28}>C_{30}) are accompanied by methylsteranes (including dinosterane) and abundant diasteranes (Edwards et al., 1998). The abundance of vanadyl relative to nickel porphyrins in these asphaltites is high ($\approx$ 22:1), and their

10

methylphenanthrene indices reveal that they were expelled from their source rock(s) at relatively low thermal maturities (calculated vitrinite reflectance, Rc = 0.68–0.75%: Table 2).

3.2 Origin of the initially discharged asphaltic bitumen

Understanding the genesis of the initially discharged asphaltic bitumen may assist in constraining the source of the southern Australian asphaltite strandings. Undoubtedly, the asphaltites have lost volatile components subsequent to their escape from the subsurface to the sea floor. This loss is likely to have involved both submarine dissolution, as evidenced by the shrinkage cracks on the upper surface of the stranded asphaltite (Fig. 2D), and subaerial evaporation, which accounts for its loss of plasticity observed once removed from the aqueous environment. The difference in distribution of bulk components between the inner and outer portions of the specimens is relatively small, as shown by the combined loss of saturated and aromatic hydrocarbons (average 5%) and the variation in the $\sum C_{10}$–C_{19}/C_{30} n-alkane ratio (average 13%). Thus, it is probable that the major proportion of the light-end loss from the parent crude oil occurred in the subsurface and that the southern Australian asphaltites were discharged into the ocean as semi-solid bitumen.

Solid bitumens comprise allochthonous, non-disseminated organic matter that may be separated into pre-oil and post-oil products. According to the classification scheme of Curiale (1986), pre-oil bitumens are early (immature) expulsion products of rich source rocks that migrate over short distances as viscous fluids, whilst post-oil bitumens are commonly viewed as remnants of altered oils which have been subjected to severe biodegradation and/or water washing. Other possible origins for post-oil bitumens include thermal maturation of previously generated oils, residues precipitated along oil migration pathways, and deasphalting of reservoired oils by gas (Curiale, 1986; Wilhelms and Larter 1994a, b; Mueller et al., 1995; Mossman and Nagy, 1996; Head et al., 2003). Such bitumens characteristically contain high proportions of NSO-compounds and asphaltenes relative to saturated and

aromatic hydrocarbons. Typical examples are tar sands (e.g. Athabasca tar sands, Canada; Orinoco heavy oil belt, Venezuela), bituminous dykes (e.g. Neuquén Basin, Argentina; Unita Basin, Utah, USA; Seridahli vein, Turkey) and tar mats in both clastic and non-clastic petroleum reservoirs (Wilhelms and Larter 1994a, b; Mueller et al., 1995; Hwang et al., 1998; Cobbold and Rossello, 2003; Head et al., 2003; Peters et al., 2005). Tar mats, which have been described on all scales from microscopic to several tens of metres in thickness, can be defined as zones in petroleum reservoirs where asphaltenes comprise up to 20–60 wt% of an oil's C_{15+} fraction (Wilhelms et al., 1994; Wilhelms and Larter, 1994a, b; Carpentier et al., 2007).

Thermal alteration of reservoired crude oils is one process that can produce heavy oil, in the form of pyrobitumen. However, the ready solubility of the asphaltites in solvents such as dichloromethane distinguishes them from reservoir pyrobitumens, which are only weakly soluble (Wilhelms and Larter, 1994b). So too does their aforementioned low thermal maturity which is characteristic of the early oil window.

Another process capable of producing heavy oil is biodegradation which leaves distinctive molecular and isotopic fingerprints in the residual crude that reflect both its initial non-degraded composition and the nature and extent of the microbial alteration (Prince and Walters, 2007). The asphaltites do show some signs of degradation, notably a significant loss of low-molecular-weight normal and cyclic alkanes. However, this is most likely due to evaporation after their stranding on the beach (and, in the case of archived specimens, possibly also during storage). Previous investigations of Australian asphaltites (Volkman et al., 1992; McKirdy et al., 1994; Padley, 1995; Edwards et al., 1998) and the data acquired in this study reveal that they have not undergone extensive in-reservoir anaerobic biodegradation. They certainly lack 25-norhopanes, which are generally (although not necessarily) found in severely biodegraded crude oils (Peters et al., 2005). Moreover, they

display no evidence of gas vesicles or gas hydrates, which are commonly observed in the Gulf of Mexico (GOM) asphaltites (Bruning et al., 2008; Schubotz et al., 2011) where the bacteria responsible for the genesis of the heavy oil produce substantial quantities of methane. Other characteristics, such as their low isoprenoid to *n*-alkane and 20S:20R ααα sterane ratios, their homophopane distributions and their lack of a well-defined unresolvable complex mixture (UCM), all support the conclusion that the asphaltites are not mainly products of severe biodegradation. This is confirmed by their position on the recently devised Manco biodegradation scale (Larter et al., 2012), which is based on the sequential removal of 'category' compound classes according to their susceptibility to bacterial alteration. The Manco number vectors of the asphaltites analysed in this study do, however, exhibit a clear anomaly. Their fractions should show a gradual and progressive removal of components through the categories, but the combined light and heavy Manco vector of 31043310000 undoubtedly highlights the involvement of another process in their degradation.

Water washing likewise leaves its own distinctive pattern of alteration on the affected crude oil. Experiments show that this alteration is most apparent in the gasoline and kerosene ranges (C_5–C_{14}) where hydrocarbons with the same carbon number are removed in the following order of decreasing solubility: aromatics > cycloalkanes > branched alkanes > *n*-alkanes (Palmer 1984, 1993; Lafargue and Barker, 1988; Kuo, 1994; Lafargue and Thiez, 1996). It is commonly difficult to differentiate the effects of biodegradation and water washing on the C_{15+} composition because they generally occur in tandem. While alkylated naphthalenes, dibenzothiophenes and phenanthrenes are susceptible to both dissolution and aerobic biodegradation (Budzinski et al., 1998), abnormally low concentrations of the C_{20} and C_{21} triaromatic steroids can be indicative of hydrologic alteration, as these species are usually not readily biodegraded (Volkman et al., 1984; Palmer, 1993; Kuo, 1994). The absence from the asphaltites of all hydrocarbons <C_{10} and low-molecular-weight aromatic species such as the

alkylbenzenes and naphthalene is consistent with the combined effects of water washing and evaporation. However, as noted by Volkman et al. (1992), the southern margin asphaltites do not show signs of extensive water washing since methylated naphthalenes and phenanthrenes would have been less abundant than observed. Dibenzothiophene and its higher homologues are also prominent and the C_{20} and C_{21} triaromatic steroids are present in concentrations similar to those of other triaromatic species (Fig. 8D). Thus, while it is conceivable that this alteration process may have played some minor role in removing their light ends, intensive water washing of these asphaltites is not evident. This is perhaps not surprising, given that the asphaltite is likely to have reached the sea floor (and ultimately the sea surface) as a plastic mass, rather than as droplets of oil. In any case, laboratory studies have shown that water washing is unlikely to be a viable mechanism for the formation of tar mats (Lafargue and Barker, 1988; Kuo, 1994). It is instructive to compare the Australian asphaltites with the bitumen that floats on the Dead Sea (Connan et al., 1992; Connan and Nissenbaum, 1994). The latter, which is solid and was probably plastic when it reached the surface, has no light ends and is not biodegraded. It corresponds to crude oil released at the sea floor by tectonism. In this pure asphalt, oxidation is minimal and devolatilization (although not water washing) has occurred.

Tar mats, the one remaining option for the genesis of the asphaltites, are common in petroleum reservoirs. The main processes leading to their formation are gas-induced deasphalting, gravity segregation of oil columns, formation water-oil interactions, oil mixing, and secondary/tertiary migration (Wilhelms and Larter, 1994b and references therein). Simply because of the physical constraints on the movement of asphaltene-rich oils, tar mats are located at permeability barriers or phase boundaries (e.g. oil-water contacts).

The biomarker profiles of the asphaltites provide no indication that they are products of in-reservoir mixing of oils of different source affinity; and, as already discussed, water washing

is unlikely to have played a part in their formation. Changes in reservoir pressure and temperature will affect asphaltene solubility, with the lowering of either parameter leading to their precipitation. Since petroleum charges in any basin generally move along paths of decreasing pressure and temperature, it would seem inevitable that asphaltenes will be deposited from oils during their migration. Tar mats are most often, but not always, identified in zones of high porosity and lateral permeability, especially along dipping carrier beds where tectonic activity has initiated secondary (and tertiary?) migration (Wilhelms and Larter, 1994b; Carpentier et al., 2007). Where the migration pathway is close to horizontal, asphaltene clusters, aggregating following precipitation, will become concentrated in the rear of the oil stringer and there undergo gravitational settling. Thus, an accumulation of heavy asphaltic bitumen (i.e. a tar mat) is left in the wake of the migrating oil stringer (Wilhelms and Larter, 1994b).

Dissolution of natural gas in reservoired oil is another means by which a significant proportion of its asphaltene fraction can be precipitated (Wilhelms and Larter 1994a; Hwang et al., 1998). For extensive asphaltene deposits to be formed in this way would require gas-invasion of a reservoir that contains oil under-saturated with respect to gas; or, alternatively, an oil pool with an existing gas cap, which subsequently undergoes deeper burial (Wilhelms and Larter, 1994b). Given the nature of the asphaltites' source-rock kerogen (S-rich Type II) and their expulsion in the early oil window (Volkman et al., 1992; Edwards et al., 1998), their hydrocarbon kitchen is highly unlikely to be significantly gas prone although elsewhwere in the basin the same source rock may have entered the gas window. In both the Ceduna Sub-basin and Otway Basin the Cretaceous sequences immediately underlying the inferred Albian marine source rocks are of deltaic/fluvio-lacustrine and fluvio-lacustrine origin, respectively (Edwards et al., 1999; Blevin and Cathro, 2008). At least in the onshore Otway Basin, these sequences host significant accumulations of gas, whilst the formations in the western Ceduna

Sub-basin are modelled as being extensively gas mature. Thus, deasphalting through gas charging from more mature, gas-prone underlying sequences is another route to the tar-mat precursors of the asphaltites.

In summary, the original crude oil destined to become stranded asphaltite is likely to have undergone substantial subsurface alteration prior to its discharge on to the sea floor. Degradation through bacterial removal and/or intensive water washing had no part in their genesis. It is probable the asphaltite originates from tar mats formed along the secondary migration pathway of the main oil charge, or through deasphalting related to gas invasion of the reservoir. The residual viscous material, already low in gasoline-range hydrocarbons, may subsequently have been stripped of the majority of its remaining light-end saturated and aromatic hydrocarbon species by water washing before exposure to the marine environment and a final episode of devolatilization.

The physical properties of the southern margin strandings appear analogous to those of asphaltic mats or volcanoes observed emanating from the sea floor at Chapopote Knoll in the GOM as low intensity seeps of heavy viscous oil (Brüning et al., 2010), except that in this instance the oil is lightly to heavily biodegraded (Schubotz et al., 2011). Here surface cracking is due to the *in situ* loss of volatiles and subsequent fragmentation of older more brittle deposits. Flow structures and lamination are evident in cored specimens. Such features have been noted in some Australasian asphaltites, including those analysed in the present study (Fig. 2A, D). Colonisation of the GOM asphalts by benthic mussels, sponges and tubeworms allowed estimation of flow ages, with surface fissures inferred to develop in about a decade. Again, similar occurrences of molluscs and annelids are a feature of some asphaltite strandings in Australia and New Zealand (Padley, 1995; Edwards et al., 1999; Fig. 2D, E). In the GOM the asphalts are, for the most part, negatively buoyant, although one freshly deposited sample was unexpectedly positively buoyant (>10° API: Brüning et al., 2010).

Tar balls smaller than the average asphaltite stranding might also commonly escape to the surface and appear similar to the bitumens observed at Coal Oil Point, California. Farwell et al. (2009) estimated sinking rates of 0.4–5 days for 1–10 cm diameter tar droplets from the Coal Oil Point slicks. Therefore, a significant number of strandings in this size range but otherwise matching the Family 4 bitumen profile might be expected along the southern coastline of Australia, which is not the case. Logan et al. (2010) favour an oil slick that formed a stable mousse before stranding as the likely formation mechanism of the asphaltites, but this would clearly not explain their substantial benthic communities nor their flow structures and laminations. Their lack of biodegradation, cited as a reason for the strandings not being sourced from tar mat seepage, can be explained by the common absence of well established bacterial communities in low intensity seeps (Wenger and Isaksen, 2002); and by the inability of bacteria to penetrate their precursor asphaltic oil mass once exposed at the seafloor. The implication of low-intensity seepage is consistent with the pattern observed for the Australian continental shelf and ascribed to low recent burial rates (Logan et al., 2010).

3.3 Marine weathering effects: comparison of biomarker distributions from inner and outer portions of stranded asphaltite

Having established that the eleven specimens in our sample suite share a common origin (see Section 4.1), the bulk, biomarker and $\delta^{13}C$ parameters of their 'fresh' interiors were compared with those of their 'weathered' surfaces (Tables 3 and 4). The observed differences, though commonly subtle due to the bulk of the heavy oil components being both immobile and not bioavailable, are used to establish their relative degrees of weathering arising from exposure to the marine environment and, by inference, their proximity to the site(s) of seafloor seepage. The obvious lack of a freshly discharged or subsurface example of asphaltite for comparison is a significant complicating factor, as is the lack of information on how long each specimen was stranded on the beach prior to its collection and analysis.

Upon entering the ocean any crude oil is exposed to a combination of weathering processes including aerobic biodegradation, water washing, photo-oxidation and evaporation (Munoz et al., 1997; Gagnon et al., 1999; Mazeas and Budzinski, 2002; Mazeas et al., 2002; Wenger and Isaksen, 2002; Peters et al., 2005; Fernandez-Alvarez et al., 2007; Wardlaw et al., 2008; Farwell et al., 2009). These processes, generally acting in concert, can alter the initial concentrations of hydrocarbons in the discharged oil at rates orders of magnitude faster than within the subsurface carrier bed or reservoir, as revealed both by laboratory experiments and field studies of spilled oils and natural seeps (Goodwin et al., 1983; Wardroper et al., 1984; Douglas et al., 1996, 2002; Munoz et al., 1997; Wenger et al., 2001; Wenger and Isaksen, 2002; Peters et al., 2005; Wardlaw et al., 2008). However, their cumulative impact on a mass of asphaltic bitumen oozing from the seabed will be much less significant.

In both subsurface and surface environments there is simultaneous degradation of all hydrocarbons irrespective of molecular weight, and it is simply the lower rates of degradation of the high-molecular-weight and more complex species that causes the illusion of sequential degradation (Head et al., 2006; Wardlaw et al., 2008). There are, however, differences in the rate at which some categories of compounds are removed, related to the bacterial colonies involved in the degradation (Goodwin et al., 1983; Wenger and Isaksen, 2002; Head et al., 2006).

3.3.1 Saturated hydrocarbon fraction

Comparison of the saturated hydrocarbon fractions of the paired sub-samples reveals subtle differences between the interior and exterior of the asphaltites (Table 3). As a proportion of the total sample, saturated hydrocarbons decrease by an average of 16%. In specimens from the Limestone Coast and southern Kangaroo Island the depletion is <10% (with the exception of sample CB-32 in which it is 15.7%). At sites more distant from the Limestone Coast, the

depletion is generally higher: west coast of Kangaroo Island, 15–32%; Eyre Peninsula, 19–33%; and New Zealand, 17–19%.

The effects of water washing and evaporation are most likely to be visible in the distributions of n-alkanes. All specimens show an apparent loss of $<C_{20}$ homologues from their outer surface. As expressed in the n-alkane ratio $\sum C_{10}–C_{19}/C_{30}$, the extent of this loss ranges from 2 to 39%. Asphaltites from the Limestone Coast and southern Kangaroo Island exhibit the greatest depletion (>10%), suggesting that strandings closest to the Morum Sub-basin undergo significantly more loss of light hydrocarbons. Sample CB-32 exhibits the largest variation between its interior and exterior, possibly indicating that the difference may be due to a long time between its stranding (unknown), collection and analysis. Within several classes of biomarker cycloalkanes, including the steranes and hopanes, certain isomers and homologues are known to be more susceptible to biodegradation than others (Goodwin et al., 1983; McKirdy et al., 1983; Peters et al., 2005). Between the inner and outer portions of the asphaltites there is a general trend of depletion of 20R relative to 20S $\alpha\alpha\alpha$ steranes (e.g. C_{29} reduces by an average of 7%). However, the C_{27} $\alpha\alpha\alpha$ 20R sterane increases slightly relative to the C_{28} and C_{29} homologues, in contrast to the general $C_{27}>C_{28}>C_{29}$ order of depletion (Peters et al., 2005). These results are consistent with only slight biodegradation of the outer surface of the specimens. It has been shown that aerobic biodegradation of crude oils causes a sequential reduction in the $C_{31}–C_{35}$ homohopanes, increasing with molecular weight. In the asphaltites there is a similar preferential degradation of C_{35} over the $C_{31}–C_{34}$ hopanes (Fig. 9), with the homohopane index decreasing by an average of 28% (range 5–41%). The greatest variation of the latter parameter is observed in the strandings furthest from the Limestone Coast, except for sample NZ1. By comparison with the outcomes of laboratory culture experiments (Goodwin et al., 1983), the stranded asphaltites appear to have had a relatively short exposure to aerobic biodegradation, possibly of the order of tens of years. At their outer

surfaces, the contribution of hopanoids to the total abundance of terpanes and steranes also diminishes by an average of 5%. Again, it is the specimens further from the Limestone Coast that generally sustain the greatest loss of hopanes, though sample NZ1 is once more an outlier.

There are a number of additional factors that may affect the aforementioned hydrocarbon distributions, such as initial time on the ocean floor before transportation to the shelf, microbial colonisation differences from location to location, and the time beached prior to collection. However, the majority of the parameters based on weathering-susceptible components of the asphaltites concur in showing that the strandings along the Limestone Coast exhibit less surficial alteration than those from elsewhere. Sample NZ1 from New Zealand appears anomalous. This specimen has an unusual laminated appearance (Fig. 2E) and the available section was quite thin (<2 cm). If the sample was actually a composite of laminar flows of discharged bitumen then our inner sub-sample may not be sufficiently deep to retain an unweathered profile. Alternatively, if the rate of extrusion was slow, each laminar flow may have been degraded before the next one.

3.3.2 Aromatic hydrocarbon fraction

The relative proportions of aromatic hydrocarbons in the exterior of the asphaltites are on average 11% less than in their interior (Table 3). No geographic trend is evident in this depletion, although there does seem to be a correlation with the degree of physical weathering (Table 1). Samples in which the loss of aromatics is >30% (e.g. CB-32, 80 and CL1) appear moderately to heavily weathered, whereas in samples described as less weathered (e.g. 27A, 162 and MH1) the loss is <12.5%. The 'weathered' sample 85 (Padley, 1995) from Kangaroo Island, with a decrease of only 7%, does not follow this pattern and both the samples from New Zealand show little difference.

Aromatic compounds are known to be susceptible in varying degrees to both photo-oxidation and biodegradation (Volkman et al., 1984; Douglas et al., 1996, 2002; Lee, 2003). Photo-oxidation experiments conducted on crude oils have been shown to deplete their bulk aromatic fractions by up to 40% (Maki et al., 2001), suggesting that it may be the major mechanism of asphaltite alteration. One such UV-sensitive aromatic species is benzo(a)pyrene (BaP), which also happens to be of low aqueous solubility and resistant to biodegradation (Douglas et al., 2002; Lee, 2003). Although a minor component, its abundance relative to the more resistant benzo(b)fluoranthene proved useful in assessing the contribution of photo-oxidation to the weathering of the asphaltites. All samples showed a depletion of BaP in the surface portion, with the difference between the inner and outer portions increasing in the order CL1>80>NZ2>CB-32 >NZ1> MH1>168>85 >27A> 177>162 (Table 3). This pattern appears to reflect both the physical weathering of the specimens and their geographic distribution. Except for sample 85, the most weathered specimens again show the larger depletion, whilst in the other samples it seems to depend on distance from the Limestone Coast. The more abundant aromatic species, phenanthrene (P) and dibenzothiophene (DBT), when normalised against their more stable alkylated homologues, revealed no discernible alteration attributable to photo-oxidation. This may be because the respective alkylated homologues, being more susceptible to biodegradation (Douglas et al., 1996; Haritash and Kaushik, 2009; Wardlaw et al., 2011), were depleted to essentially the same extent as P and DBT, albeit by a different mechanism.

With the majority of the water-soluble, low-molecular-weight aromatic species, such as the BTEX (benzene, toluene, ethyl benzene and xylene isomers) and naphthalenes (Palmer, 1993; Douglas et al., 1996), having probably been removed from the asphaltic bitumens prior to their marine exposure, the consequences of further water washing are likely to be minor. Biodegradation also appears to be relatively minor. It is worth noting that there is no

difference between the Manco numbers generated from the inner and outer (weathered) portions of these asphaltites. Thus, a variety of factors could be influencing the weathering patterns of the aromatic hydrocarbons, with photo-oxidation possibly having the greatest impact.

3.3.3 *n*-Alkane carbon isotopic profiles

The C_{15}–C_{31} *n*-alkanes of the asphaltites are isotopically light, with $\delta^{13}C$ values falling between –33.3 and –36.9‰ (Table 4). The difference between the values of the same homologue in their inner and outer portions varies systematically according to their geographic location (Fig. 10). Individual *n*-alkanes show >1‰ depletion of ^{13}C in the weathered exterior of the New Zealand and Eyre Peninsula asphaltites, whereas the Limestone Coast specimens deviate by <±0.4‰ and those from Kangaroo Island are generally enriched in ^{13}C by >0.5‰. Analytical precision is ±0.4‰ or better, so the greater difference observed for the Kangaroo Island, Eyre Peninsula and New Zealand strandings must be due to weathering, especially given that they have essentially the same thermal maturity (Table 2). Unlike the *n*-alkane $\delta^{13}C$ *versus* carbon number profiles previously reported for southern Australian asphaltites (Dowling et al., 1995; Edwards et al., 1998), those of the present sample suite (Fig. 10) are flat (instead of concave upward) and offset to lighter values by ~2‰. While the difference in shape may be due to more intense weathering of the original samples, the latter feature is attributable to the fact that the earlier analyses were performed more than 12 years ago and on a different system which yielded less accurate results. This is substantiated by the fact that one of the original samples was re-analysed as part of the present study (viz. CB 32 from Beachport: Table 1).

Isotopic values of petroleum hydrocarbons have been deemed to be fairly conservative under the influence of weathering (Sofer 1984; Mazeas et al., 2002; Philp et al., 2002; Schmidt et al, 2004; Hough et al., 2005; Jeffery, 2007), so the narrow range of variation per homologue (–

2.0 to 1.9‰) is to be expected. During biodegradation, the slightly faster cleavage of $^{12}C–H$

bonds results in an accumulation of molecules with $^{13}C–H$ in the remaining substrate

(Bouchard et al., 2008; Asif et al., 2009; Hofstetter and Berg, 2011). The magnitude of the

enrichment decreases with increasing number of carbon atoms, a trend that can partly be

explained by the decreasing probability of a ^{13}C atom being located at the reaction site in the

molecule as chain length increases. Such a trend is not evident in the outer n-alkane $\delta^{13}C$

profiles of any of the asphaltites displaying net ^{13}C-enrichment (Fig. 10C). These specimens

(viz. those from Kangaroo Island and one from the Limestone Coast) might otherwise be

interpreted as displaying evidence of aerobic biodegradation before and after stranding.

The factors affecting abiotic weathering of crude oil are unclear. Sofer (1984) highlighted the

fact that the C-isotopic composition of crude oils can be altered by water washing and Palmer

(1996) cited examples from the Philippines where the saturated hydrocarbon fraction became

depleted in ^{13}C, resulting in an isotopically lighter oil. Hence, it may be as a result of their

longer residency in the marine environment that n-alkanes in the exterior portions of the Eyre

Peninsula and New Zealand asphaltites show the greatest depletion in ^{13}C.

3.4 Location of parent petroleum system

3.4.1 Imported artefacts or products of local seepage?

The close proximity of common stranding sites to the locations of former whaling stations

raises the possibility of an anthropogenic origin for the asphaltites. According to one early

commentator (Wade, 1915) tars used for caulking the wooden boats employed in the industry

were buried on beaches, whilst many cargo vessels were lost en-route to supplying the

aforementioned stations. These lost cargoes or the erosion of cached barrels during storms

would be a viable explanation. However, an investigation of the pine and coal tars recovered

from 17th, 18th and 19th century shipwreck sites, and identified as being the common caulking

materials brought into the region, showed that they differ significantly in composition from

the asphaltites, thus excluding such industrially transported materials as their source (Smart, 1999). The use of locally sourced caulking materials is confirmed in historical records of the early settlement of southern Australia (e.g. Tolmer, 1882). Distribution of this pitch by the whaling fleet could account for its wide dispersal to other whaling communities (Boult et al., 2005), although it should be noted that there are no reports of asphaltite having been found adjacent to such communities along the eastern seaboard of Australia.

We are therefore left with the probability that the asphaltites are of local origin. Several offshore sedimentary basins along Australia's southern continental margin have been variously evaluated as possible hosts for the asphaltites' parent petroleum system (Fig. 1B). Of these, the two most likely to contain the required euxinic marine source rock of Late Mesozoic age are the eastern Bight Basin and the western Otway Basin (Fig. 4). An important clue to the likely origin of the asphaltites is the striking similarity of their biomarker and isotopic signatures to those of the upper Albian Toolebuc Formation in the onshore Eromanga Basin (Boreham et al., 2001). Coeval units deposited along the Blue Whale Seaway (Fig. 3), which may well host their enigmatic source facies, form part of the post-rift sag phase succession of the Blue Whale Supersequence in the Eyre and Ceduna sub-basins of the Bight Basin and the Otway Supergroup in the Otway Basin (Totterdell et al., 2000, 2008; Boreham et al., 2001, Struckmeyer et al., 2001; Bradshaw et al., 2003, Totterdell and Struckmeyer, 2003; Boult et al., 2005; Blevin and Cathro, 2008).

3.4.2 Eastern Bight Basin

Located along the southern edge of the Madura Shelf in the eastern Bight Basin, the Eyre and Duntroon sub-basins (Fig. 5A) are perched rift basins consisting of a Middle Jurassic–Early Cretaceous half graben overlain by a comparatively thin cover of sag phase sediments (Espurt et al., 2009). At Jerboa-1 in the Eyre Sub-basin (Fig. 1B), organic-rich Blue Whale sediments are geochemically distinct from the asphaltites and the minor oil shows and fluid inclusion

oils exhibit a lacustrine source affinity (Edwards et al., 1999; Ruble et al., 1999; 2001).

However, further east in the Ceduna Sub-basin (Fig. 1B), oil shows found in Cretaceous sands

at Greenly-1 have been assigned to two genetic families (Smith and Donaldson, 1995), one of

which has a biomarker distribution indicative of its origin from a calcareous anoxic marine

source rock containing a mixture of algal and land-plant organic matter (Edwards et al.,

1999). This inferred source facies may be the proximal expression of a deep-water organic

facies, located further offshore in the Ceduna Sub-basin (Fig. 5A, B), that lacks terrestrial

plant input and therefore qualifies as a potential source of the asphaltites. Additional support

for this idea is provided by Boreham et al. (2001), whose analysis of an organic-rich

mudstone (3.1% TOC) from a thermally immature Blue Whale succession penetrated by the

drill hole Eyre-1 in the onshore Bight Basin (Figs. 1B and 3) revealed a close match between

its source and age-specific biomarkers and those of the asphaltites.

A subsequent survey of the Ceduna Sub-basin by Geoscience Australia (survey SS01/2007)

identified a number of potential areas for natural seepage based on remote sensing

observations. During the survey 259 dredge, core and grab samples were collected, primarily

from the seaward edge of the Eyre Terrace where canyon formation, slumping and faulting

have exposed an interpreted mid-Cretaceous (Albian to Santonian) stratigraphic section (Fig.

5B: Totterdell et al., 2008). Screening of these specimens identified some as excellent

potential source rocks (up to 6.2% TOC and 479 mg HC/g TOC) of late Cenomanian–early

Turonian age, albeit thermally immature. Thirty high-graded samples from the Blue Whale,

White Pointer and Tiger Super sequences (Fig. 4) show biomarker distributions closely

related to those of the asphaltites. However, subtle but significant differences (viz. Ni>V

rather than V>Ni metalloporphyrins and an absence of isorenieratane) indicate that these

samples were deposited under more oxic conditions than the asphaltite source rock (Summons

and Powell, 1986; Grice et al., 1996, 1997). Nevertheless, some variation of depositional

conditions is to be expected within a given petroleum system and local 'sweet spots', such as those indicated by seismic mapping down dip from sampling sites, may be the elusive source zone (Totterdell et al., 2008). These potential source rocks in the western Ceduna Sub-basin presently lie within the gas window or are over-mature, except along the outer edge, with modelling suggesting that any Blue Whale-derived hydrocarbons are likely to be gas accumulations (Fig. 5B, C). In the eastern section of the basin the same sequences are still within the oil generation window.

Along the upper slope and shelf-break canyons of the eastern Ceduna Sub-basin there is evidence of hydrocarbon seeps from sniffer, synthetic aperture radar (SAR) and airborne laser fluorescence (ALF) data, whilst 2D seismic data appear to show pocks, sea floor mounds, upturned reflectors at depth and depressed shallow reflectors within Cenozoic sediments that represent recent or currently active fluid escape features on the shelf (Struckmeyer et al., 2002; Hillis and Reynolds, 2003; Totterdell et al., 2008; Logan et al., 2010; Boult, 2012). However, neither sea floor tar mats nor asphaltic volcanoes have yet been identified.

3.4.3 Western Otway Basin

Within the western Otway Basin, the offshore Morum Sub-basin (Fig. 6A) likewise exhibits good potential to host the asphaltite source facies. The long history and high concentration of asphaltite strandings along the adjacent shoreline have been regarded as evidence of their local origin (Sprigg and Woolley, 1963; Sprigg, 1986; McKirdy et al., 1994). The apparent temporary increase in strandings following local earthquake activity and the large quantities collected after severe storm events, such as in 1961 when Sprigg and associates retrieved 'almost half a ton' south of Kingston (Fig. 7), also suggest proximity to the parent petroleum system (Sprigg and Woolley, 1963; McKirdy et al., 1994; Boult et al., 2005).

The Otway Basin, like the Bight Basin, comprises a series of graben and half graben filled with Jurassic to Lower Cretaceous rift sediments (Boult and Hibburt, 2002). The rate of

26

rifting slowed during the Barremian to Albian but rapidly increased before the end of the Albian in the northern part of the basin, with extension rate studies suggesting deposition of marine sediments in the Morum Sub-basin corresponding in age to the Albian OAE (Palmowski et al., 2004; Boult et al., 2005). The widespread Cenomanian unconformity mapped in the onshore is predicted not to extend into the Morum Sub-basin, where over 4 km of upper Albian to Lower Cretaceous sediments are preserved (Boult and Hibburt, 2002). A potential Albian OAE source pod has been interpreted from seismic data (Fig. 6B) along with amplitude anomalies, diapiric structures and possible gas chimneys (Boult et al., 2005). Here canyons cut deeply (up to 1.6 km) into the stratigraphic section on the continental slope, exposing Cainozoic to Lower Cretaceous strata and coinciding with SAR anomalies that are possibly indicative of light hydrocarbon seepage to the sea surface (Fig. 7).

Further north at Troas-1 on the Chama Terrace (Figs. 1C and 6B), the basal Eumeralla Formation of Aptian age has attained maturities of R_o ~0.5–0.7% (Padley, 1995), so the maturation level of R_o ~0.75% required for the inferred upper Albian marine shales to be capable of sourcing the asphaltites is not unreasonable. As their generation and expulsion from the source rock would have occurred quite early in the basin's history (Boult and Hibburt, 2002), the initial oil charge may have been to sub-horizontal carrier beds conducive to tar mat formation. Subsequent structural development of the prominent steeply dipping and inverted faults observed within the sub-basin may then have facilitated the continued migration of the lighter hydrocarbons to reservoirs higher in the sequence, where diapiric structures and gas chimneys have been interpreted (Boult et al., 2005), leaving behind residual tar mats. Later, this heavy bitumen could have been exposed by the erosion of the canyon into the reservoir facies and now be slowly extruding to the sea floor under limited buoyancy from its contact with seawater. This would explain the low amplitude of the seep inferred from the asphaltite's physical characteristics. Loss of the low concentrations of gasoline-range

hydrocarbons, evidenced by the shrinkage cracks on the asphaltites, would also help explain the SAR anomalies over the canyon (Fig. 7).

In summary, on the basis of our present knowledge of the eastern Bight Basin and the western Otway Basin, both are ideal candidates for the role of sourcing the asphaltites. The west-to-east rifting and subsequent separation of Australia from Antarctica would have created suitable depocentres for their source rocks, the well-documented OAEs of this period of Earth history providing the required depositional conditions implicit in their source and age-specific biomarker signatures.

3.5 Asphaltite dispersal pattern

Although the largest reported specimens are those described by Hills (1914) from the west coast of Tasmania, there is strong historical evidence for asphaltite being stranded upon the shores of the western Otway Basin in higher concentration than elsewhere along Australia's southern margin (Fig. 1A: Sprigg and Woolley, 1963). By itself, this is suggestive of a local source. The new data presented herein show that the least weathered asphaltites strand along the Limestone Coast of the western Otway Basin, as opposed to Kangaroo Island or the Eyre Peninsula. This finding is consistent with their origin from seepage sites located within the submarine canyons of the Morum Sub-basin. Boult et al. (2005) postulated that oil seepage into these shelf- break canyons or the nearby slope may form asphaltic mats, which are periodically dislodged and transported up the canyons to the shelf by the Bonney Upwelling of the cold, deep-water Flinders Current (Fig. 7).

The summer upwelling of the Flinders Current is known to focus water flow up the Bonney canyons (Middleton and Bye, 2007) where water velocities are likely to be of the same order as those measured in the Astoria shelf-break canyon off the coast of Oregon ($0.1–0.2$ m s^{-1}: Kämpf, 2007). Such water flow is more than sufficient to transport asphaltite onto the shelf. Earthquakes, which are common in the region, may exacerbate natural fracturing of the tar

mats and dislodge fragments into the water column. They have certainly been noted to temporarily increase the frequency of coastal bitumen strandings (Sprigg and Woolley, 1963). Once transferred to the shelf the asphaltites can be driven onto the local coastline by waves or carried westward by the Flinders Current (Middleton and Platov, 2003). Alongshore, this current moves past Kangaroo Island and into the Great Australian Bight during periods of upwelling. Its velocity can exceed 50 cm s^{-1} with potential advection estimated at up to 800 km over a three-month period (Middleton and Bye, 2007). This strong current, in concert with local storm-driven wave activity, could deposit asphaltite along the southern and western shores of Kangaroo Island. The Flinders Current may also drive the distribution further westward along the base of the shelf, thereby explaining the less frequent occurrences of asphaltite stranding in Western Australia. Water flow off the shelf will likewise focus down the canyon and sweep non-buoyant bitumen onto the abyssal plane, where it can be transported to the west. Prevailing southwesterly weather patterns can account for the transport over the narrow shelf where strong storm conditions have been associated with an increase in bitumen stranding, as in May/June 1961when Sprigg and associates collected 'almost half a ton' in the weeks following the first storm of the winter season (Sprigg and Woolley, 1963). For most of the year the prevailing current across the shelf is actually the easterly coastal current (Middleton and Bye, 2007). This warmer, surface current flows along the full length of the southern margin out past Tasmania towards the Southern Ocean, where it can interact with the prevailing Subantarctic Front of the Antarctic Circumpolar Current system (Rintoul et al., 2001). A study by Bye (1988) showed that drift cards placed in the Antarctic Circumpolar Current eventually stranded on the shores of New Zealand. Therefore the coastal current is a likely mechanism for distribution of asphaltite to the shores of Tasmania, and beyond to New Zealand and Macquarie Island (Fig. 1A).

In the eastern Ceduna Sub-basin, the strong evidence of seepage from its petroleum systems onto the shelf and the availability of the Flinders Current transport mechanism during the summer months are sufficient to make this area another prospective source for the asphaltites. Moreover, there is anecdotal evidence of asphaltite stranding being common at nearby Sleaford Bay and other localities on the southern Eyre Peninsula (Sprigg and Woolley (1963). If a mid-Cretaceous source pod had been active, as seems likely from basin modelling (Boult, 2012), and migration of the resulting oil stringer deposited an asphaltic tar mat, the only remaining problem is that shelf-break canyons do not appear to expose the Cretaceous section in this part of the sub-basin. Further west, upper-slope canyons do incise the Cretaceous sequence, and the molecular and isotopic signatures of one of its organic-rich units are remarkably similar to those of the asphaltites. However, unless the freshly exposed tar mat is sufficiently buoyant to rise through the water column to the surface, there is no obvious mechanism for the transfer of asphaltite from these deep-water westerly zones up onto the shelf. The shallow coastal current will provide no up-canyon fluid flow whilst the Flinders Current, which upwells to the south during the summer, circulates back off the shelf in the western Ceduna Sub-basin (Middleton and Bye, 2007).

4. Conclusions

Geochemical investigation of four previously unanalysed asphaltites from locations in western South Australia and the south island of New Zealand has shown that these more distant strandings may be correlated with a further seven members of the classic 'Family 4' asphaltites recovered from sites of stranding on Kangaroo Island and along the Limestone Coast of South Australia. Comparison of inner, fresher portions of each stranding to their outer, weathered surface section revealed differences in several degradation-sensitive components. Molecular fossil and compound-specific $\delta^{13}C$ signatures in the saturated hydrocarbons most susceptible to alteration by biodegradation and dissolution suggest that the

specimens recovered from the Eyre Peninsula and New Zealand have had longer exposure to weathering in the oceanic realm than those from the Limestone Coast and Kangaroo Island. The corresponding aromatic hydrocarbon distributions of the inner and outer portions differ in a manner consistent with the physical appearance of the strandings.

The levels of degradation displayed by the asphaltites highlight the fact that the parent crude oil has undergone substantial alteration. Given its arrival at the sea floor in the form of heavy oil, this modification must have occurred in the subsurface. The most likely mechanism is tar mat formation, probably due to deasphalting along a flat-lying migration pathway during secondary migration of the main oil stringer or through deasphalting related to gas invasion of the reservoir. Apart from their obvious lack of severe biodegradation, a characteristic they share with the famous Dead Sea asphalt, the Australasian asphaltites otherwise exhibit many of the hallmarks of the viscous bitumen issuing from the seafloor as asphaltic volcanoes in the Gulf of Mexico.

These Australasian asphaltites appear to be products of low-intensity seeps in the Ceduna Sub-basin of the Bight Basin, where suitable mid-Cretaceous marine potential source rocks have been identified, and/or the Morum Sub-basin of the Otway Basin offshore from the Limestone Coast and southern Kangaroo Island, where the least weathered asphaltites in this study stranded and the highest concentration of historical strandings is recorded. Before their degree of weathering can be equated to distance travelled from their parent seafloor seep(s), a similar follow-up study, based on *freshly stranded* asphaltites from the same localities, is needed to minimise the effects of subaerial exposure and oxidation.

5. Acknowledgements

6. References

Ahmed, M., George, S.C., 2004. Changes in the molecular composition of crude oils during their preparation for GC and GC-MS analyses. Organic Geochemistry 35, 137–155.

Asif, M., Grice, K., Fazeelat, T., 2009. Assessment of petroleum biodegradation using stable hydrogen isotopes and polycyclic aromatic hydrocarbons. Organic Geochemistry 40, 301–311.

Blevin, J.E., Cathro, D., 2008. Australian Southern Margin Synthesis – GA707

https://www.ga.gov.au/products/servlet/controller?event=GEOCAT_DETAILS&catno=68892

Blevin, J.E., Totterdell, J.M., Logan, G.A., Kennard, J.M., Struckmeyer, H.I.M., Colwell, J.B., 2000. Hydrocarbon prospectively of the Bight Basin—petroleum systems analysis in a frontier basin. Geological Society of Australia, Abstracts 60, 24–29.

Boreham, C.J., 2008. Bight Basin marine potential source rocks: a local expression of the Late Cretaceous oceanic anoxic event (OAE2)? In: McKirdy, D.M. (Ed.), Oil, Soil, Water and Wine. 15th Australian Organic Geochemistry Conference, Program and Abstracts, 104–105.

Boreham, C.J., Krassay, A.A., Totterdell, J.M., 2001. Geochemical comparisons between asphaltites on the southern Australian margin and Cretaceous source rock analogues. In: Hill, K.C., Bernecker, T. (Eds.), Eastern Australasian Basins Symposium: A refocused energy perspective for the future. Petroleum Exploration Society of Australia, Special Publication, pp. 531–541.

Bouchard, D., Hunkeler, D., Höhener, P., 2008. Carbon isotope fractionation during aerobic biodegradation of *n*-alkanes and aromatic compounds in unsaturated sand. Organic Geochemistry 39, 23–33

Boult, P.J., Hibburt, J.E., 2002. The Petroleum Geology of South Australia. Volume 1: Otway Basin. 2nd edition. South Australia. Department of Primary Industries and Resources.

Boult, P.J., McKirdy D., Blevin J., Heggeland R., Lang S., Vinall D., 2005. The oil-prone Morum Sub-basin petroleum system, Otway Basin, South Australia. MESA Journal 38, 28–33.

Boult, P.J., 2012. Bight Basin Overview. http://www.bightpetroleum.com/bight-basin/overview

Bradshaw, B.E., Rollet, N., Totterdell, J.M., Borissova, I., 2003. A revised structural framework for frontier basins on the southern and south-western Australian continental margin. Geoscience Australia Record 2003/03.

Brüning, M., Sahling, H., MacDonald, I., Ding, F., Bohrmann, G., 2010. Origin, distribution, and alteration of asphalts at the Chapopote Knoll, southern Gulf of Mexico. Marine and Petroleum Geology 27, 1093–1106.

Budzinski, H., Raymond, N., Nadalig, T., Gilewicz, M., Garrigues, P., Bertrand, J.C., Caumette, P., 1998. Aerobic biodegradation of alkylated aromatic hydrocarbons by a bacterial community. Organic Geochemistry 28, 337–348.

Bye, J.A.T., 1988. Drift cards in the southern ocean and beyond (1972-1988). Flinders Institute for Atmospheric and Marine Sciences, Flinders University of South Australia. Cruise Report No. 14.

Carpentier, B., Arab, H., Pluchery, E., Chautru, J.M., 2007. Tar mats and residual oil distribution in a giant oil field offshore Abu Dhabi. Journal of Petroleum Science and Engineering 58, 472–490.

Cobbold, P.R., Rossello, E.A., 2003. Aptian to recent compressional deformation, foothills of the Neuque´n Basin, Argentina. Marine and Petroleum Geology 20, 429–443.

Connan, J., Nissenbaum, A., Dessort, D., 1992. Molecular archaeology: Export of Dead Sea asphalt to Canaan ad Egypt in the Chalcolithic–Early Bronze Age (4th–3rd millennium BC). Geochimica et Cosmochimica Acta 56, 2743–2759.

Connan, J., Nissenbaum, A., 2004. The organic geochemistry of the Hasbeya asphalt (Lebanon): comparison with asphalts from the Dead Sea area and Iraq. Organic Geochemistry 35, 775–789.

Curiale, J. A., 1986. Origin of solid bitumens, with emphasis on biological marker results. Organic Geochemistry 10, 559-580.

Currie T.J., Alexander R., Kagi R.I., 1992. Coastal bitumens from Western Australia – long distance transport by ocean currents. Organic Geochemistry 18, 595–601.

Dawson, D., Grice, K., Alexander, R., Edwards, D., 2007. The effect of source and maturity on the stable isotopic compositions of individual hydrocarbons in sediments and crude oils from the Vulcan Sub-basin, Timor Sea, Northern Australia. Organic Geochemistry 38, 1015–1038.

Douglas, G.S., Bence, E., Prince, R.C., McMillen, S.J., Butler, E.L., 1996. Environmental stability of selected petroleum hydrocarbon source and weathering ratios. Environmental Science & Technology 30, 2332–2339.

Douglas, G.S., Owens, E.H., Hardenstine, J., Prince, R.C., 2002. The OSSA II Pipeline oil spill: the character and weathering of the spilled oil. Spill Science & Technology Bulletin 7, 135–148.

Dowling, L.M., Boreham, C.J., Hope, J.M., Murray, A.P., Summons, R.E., 1995. Carbon isotopic composition of hydrocarbons in ocean-transported bitumens from the coastline of Australia. Organic Geochemistry 23, 729–737.

Edwards D., McKirdy D.M., Summons R.E., 1998. Enigmatic asphaltites from the southern Australian margin: molecular and carbon isotopic composition. PESA Journal 26, 106–130.

Edwards, D.S., Struckmeyer, H.I.M., Bradshaw, M.T., Skinner, J.E., 1999. Geochemical characteristics of Australia's Southern Margin petroleum systems. Australian Petroleum Production and Exploration Association Journal 39, 297–321.

Espurt, N., Callot, J., Totterdell, J., Struckmeyer, H., Vially, R., 2009. Interactions between continental breakup dynamics and large-scale delta system evolution: Insights from the Cretaceous Ceduna delta system, Bight Basin, Southern Australian margin, Tectonics 28, 1–26.

Farwell, C., Reddy, C.M., Peacock, E., Nelson, R.K., Washburn, L., Valentine, D.L., 2009. Weathering and the fallout plume of heavy oil from strong petroleum seeps near Coal Oil Point, CA. Environmental Science and Technology 43, 3542–3548.

Fernandez-Alvarez, P., Vila, J., Garrido, J.M., Grifoll, M., Feijoo, G., Lema, J.M., 2007. Evaluation of biodiesel as bioremediation agent for the treatment of the shore affected by the heavy oil spill of the Prestige. Journal of Hazardous Material 147, 914–922.

Gagnon, M.M., Grice, K., Kagi, R.I., 1999. Biochemical and chemical parameters for aquatic ecosystem health assessments adapted to the Australian oil and gas industry. Australian Petroleum Production and Exploration Association Journal 39, 584–598.

Goodwin N.S., Park P.J.D., Rawlinson A.P., 1983. Crude oil biodegradation under simulated and natural conditions. In: Björoy, M., (Ed.), Advances in Organic Geochemistry 1981, Wiley, Chichester, pp. 650–658.

Grice, K., Alexander, R., Kagi, R.I., 2000. Diamondoid hydrocarbon ratios as indicators of biodegradation in Australian crude oils. Organic Geochemistry 31, 67–73.

Grice. K., Schaeffer, P., Schwark, L., Maxwell, J.R., 1996. Molecular indicators of the palaeoenvironmental conditions in an immature Permian shale (Kupferschiefer, Lower Rhine Basin, north-west Germany) from free and S-bound lipids. Organic Geochemistry 25, 131–147.

Grice. K., Schaeffer, P., Schwark, L., Maxwell, J.R., 1997. Changes in palaeoenvironmental conditions during deposition of the Permian Kupferschiefer (Lower Rhine Basin, northwest Germany) inferred from molecular and isotopic compositions of biomarker components. Organic Geochemistry 26, 677–690.

Hallmann, C., Schwark, L., Grice, K., 2008. Community dynamics of anaerobic bacteria in deep petroleum reservoirs. Nature Geoscience 1, 588–591.

Haritash, A.K., Kaushik, C.P., 2009. Biodegradation aspects of polycyclic aromatic hydrocarbons (PAHs): A review. Journal of Hazardous Materials 169, 1-15.

Hartman, B.H., Hammond, D., 1981. The use of carbon and sulfur isotopes as correlation parameters for the source identification of beach tar in the southern California borderland. Geochimica et Cosmochimica Acta 45, 309–319.

Head, I.M., Jones, D.M., Larter, S.R., 2003. Biological activity in the deep subsurface and the origin of heavy oil. Nature 426, 344–352.

Head I.M., Jones D.M., Röling W.F.M., 2006. Marine microorganisms make a meal of oil. Nature Reviews: Microbiology 4, 173–182.

Hills, L., 1914. Geological reconnaissance of country between Cape Sorrell and Point Hibbs. Geological Survey of Tasmania Bulletin 18.

Hillis, R.D., Reynolds, S.D., 2003. In situ stress field, fault reactivation and seal integrity in the Bight Basin. South Australia. Department of Primary Industries and Resources. Report Book 2003/2.

Hofstetter, T.B., Berg, M., 2011 Assessing transformation processes of organic contaminants by compound-specific stable isotope analysis. Trends in Analytical Chemistry 30, 618–627.

Hough, R.L., Whittaker, M., Fallick, A.E., Preston, T, Farmer, J.G., Pollard, S.J.T., 2005. Identifying source correlation parameters for hydrocarbon wastes using compound-specific isotope analysis. Environmental Pollution 143, 489–498.

Hwang, R.J., Teerman, S.C., Carlson, R.M., 1998. Geochemical comparison of reservoir solid bitumens with diverse origins. Organic Geochemistry 29, 505–517.

Jeffery, A.W.A., 2007. Application of stable isotope ratios in spilled oil identification. In: Wang, Z., Stout, S.A. (Eds.), Oil Spill Environmental Forensics: Fingerprinting and Source Identification. Academic Press, Burlington, MA, pp. 207–227.

Jenkyns, H.C., 2010. Geochemistry of oceanic anoxic events. Geochemistry, Geophysics, Geosystems 11, 1–30.

Jones, D.M., Head, I.M., Gray, N.D., Adams, J.J., Rowan, A.K., Aitken, C.M., Bennett, B., Huang, H., Brown, A., Bowler, B.F.J., Oldenburg, T., Erdmann, M., Larter, S.R., 2008. Crude-oil biodegradation via methanogenesis in subsurface petroleum reservoirs. Nature 451, 176–180.

Kämpf, J., 2007. On the magnitude of upwelling fluxes in shelf-break canyons. Continental Shelf Research 27, 2211-2223.

Kuo, L.C., 1994. An experimental study of crude oil alteration in reservoir rocks by water washing. Organic Geochemistry 21, 465–479.

Lafargue, E., Barker, C., 1988. Effect of water washing on crude oil composition. American Association of Petroleum Geologists Bulletin 72, 263–276.

Lafargue, E., Le Thiez, P., 1996. Effect of water washing on light ends compositional heterogeneity. Organic Geochemistry 24, 1141–1150.

Larter, S.R., Gates, I., Adams, J., Bennett, B., Huang, H., Koksalan, T., Fustic, M., 2006a. Reservoir fluid characterization of tar sand and heavy oil reservoirs - impact of fluid heterogeneity on production characteristics. American Association of Petroleum Geologists 2006 Annual Convention – Perfecting the Search – Delivering on Promises, April 9–12. George R. Brown Convention Center, Houston, Texas, USA.

Larter, S.R., Huang, H., Adams, J.J., Bennett, B., Jokanola, O., Oldenburg, T.B.P., Jones, M., Head, I.M., Riediger, C.L., Fowler, M.G., 2006b. The controls on the composition of biodegraded oils in the deep subsurface. Part II – geological controls on subsurface biodegradation fluxes and constraints on reservoir-fluid property prediction. American Association of Petroleum Geologists Bulletin 90, 921–938.

Larter, S.R., Huang, H., Adams, J.J., Bennett, B., Snowdon, L.R., 2012. A practical biodegradation scale for use in reservoir geochemical studies of biodegraded oils. Organic Geochemistry 45, 66–76.

Lee, R.F., 2003. Photo-oxidation and photo-toxicity of crude and refined oils. Spill Science & Technology Bulletin 8, 157–162.

Logan, G.A., Jones, A.T., Kennard, J.M., Ryan, G.J., Rollet, N., 2010. Australian offshore natural hydrocarbon seepage studies, a review and re-evaluation. Marine and Petroleum Geology 27, 26–45.

Maki, H., Sasaki, T., Harayama, S., 2001. Photo-oxidation of biodegraded crude oil and toxicity of the photo-oxidized products. Chemosphere 44, 1145-1151.

Mazeas, L., Budzinski, H., Raymond N., 2002. Absence of stable carbon isotope fractionation of saturated and polycyclic aromatic hydrocarbons during aerobic bacterial biodegradation. Organic Geochemistry 33, 1259–1272.

Mazeas, L., Budzinski H., 2002. Molecular and Stable Carbon Isotopic Source Identification of Oil Residues and Oiled Bird Feathers Sampled along the Atlantic Coast of France after the Erika Oil Spill. Environmental Science & Technology 36, 130–137.

McGowran, B., Li, Q., Cann, J., Padley, D., McKirdy, D. M., Shafik, S., 1997. Biogeographic impact of the Leeuwin Current in southern Australia since the late middle Eocene. Palaeogeography, Palaeoclimatology, Palaeoecology 136, 19–40.

McKirdy, D.M., 1984a. Coastal bitumens and potential source rocks in the western Otway Basin, South Australia and Victoria. AMDEL Report F5840/84 for Australian Aquitaine Petroleum Pty Ltd. and Ultramar Australia Inc.

McKirdy, D.M., 1984b. Coastal bitumen and potential source rocks, Duntroon Basin. South Australia. AMDEL Report F5769/84 for Getty Oil Development Co. Ltd.

McKirdy, D. M., Horvath, Z., 1976. Geochemistry and significance of coastal bitumen from southern and northern Australia. Australian Petroleum Exploration Association Journal 16(1), 123–136.

McKirdy, D.M., Aldridge, A.K., Ypma, P.J.M., 1983. A geochemical comparison of some crude oils from pre-Ordovician carbonate rocks. In: Björoy, M. (ed.), Advances in Organic Geochemistry 1981, Wiley, Chichester, pp. 99–107.

McKirdy, D.M., Cox, R.E., Volkman, J.K. and Howell, V.J., 1986a. Botryococcane in a new class of Australian non-marine crude oils. Nature 320, 57–59.

McKirdy, D.M., Cox, R.E., Volkman, J.K., Howell, V.J., 1986b. Biological marker, isotopic and geological studies of lacustrine crude oils in the western Otway Basin, South Australia.

In: Fleet, A.J., Kelts, K., Talbot, M.R. (Eds.), Lacustrine Petroleum Source Rocks. Geological Society of London, Special Publication 40, 327.

McKirdy, D.M., Summons, R.E., Padley, D., Serafini, K.M., Boreham, C.J., Struckmeyer, H.I.M., 1994. Molecular fossils in coastal bitumens from southern Australia: signatures of precursor biota and source rock environments. Organic Geochemistry 21, 265–286.

Middleton, J.F., Platov, G., 2003. The mean summertime circulation along Australia's southern shelves: a numerical study. Journal of Physical Oceanography 33, 2270–2287.

Middleton, J.F., Bye, J.A.T., 2007. A review of the shelf-slope circulation along Australia's southern shelves: Cape Leeuwin to Portland. Progress in Oceanography 75, 1–41.

Mossman, D., Nagy, B., 1996. Solid bitumens: an assessment of their characteristics, genesis, and role in geological processes. Terra Nova 8, 114–128.

Mueller, E., Philp, R.P., Allen, J., 1995. Geochemical characterization and relationship of oils and solid bitumens from SE Turkey. Journal of Petroleum Geology 18, 289–308.

Munoz, D., Guiliano, M., Doumenq, P., Jacquo, F., Scherreri, P., Mille, G., 1997. Long term evolution of petroleum biomarkers in mangrove soil (Guadeloupe). Marine Pollution Bulletin 34, 868–874.

Padley, D., McKirdy, D.M., Murray, A.P., Summons, R.E., 1993. Oil strandings on the beaches of Southern Australia: origins from natural seepage and shipping. In: Øygard, K. (Ed.), Poster Sessions from the 16th International Meeting on Organic Geochemistry 20-24 September 1993, Stavanger, Norway, pp. 660–663.

Padley, D., 1995. Petroleum geochemistry of the Otway Basin and the significance of coastal bitumen strandings on adjacent southern Australian beaches. PhD Thesis, University of Adelaide.

Palmer, S.E., 1984. Effect of water washing on C_{15+} hydrocarbon fraction of crude oils from Northwest Palawan, Philippines. American Association of Petroleum Geologists Bulletin 68, 137–149.

Palmer, S. E., 1993. Effect of biodegradation and water washing on crude oil composition. In: Engel, M.H., Macko, S.A. (Eds.), Organic Geochemistry, Plenum Press, New York, pp. 511–533.

Palmowski, D., Hill, K.C., Hoffman, N., 2004. Structural-stratigraphic styles and evolution of the offshore Otway Basin - a structural seismic analysis. In: Boult, P.J., Johns, D.R., Lang, S.C. (Eds.), Eastern Australasian Basins Symposium II, Petroleum Exploration Society of Australia, Special Publication, pp. 75–96.

Pancost, R.D., Crawford, N., Magness, S., Turner, A., Jenkyns, H.C., Maxwell, J.R., 2004. Further evidence for the development of photic-zone euxinic conditions during Mesozoic oceanic anoxic events. Journal of the Geological Society 161, 353–364.

Peters, K.E., Moldowan, J.M., 1993. The Biomarker Guide - Interpreting Molecular Fossils in Sediments and Petroleum. Prentice-Hall, New Jersey.

Peters K.E., Walters C.C., Moldowan J.M., 2005. The Biomarker Guide, Volume 2, Biomarkers and Isotopes in Petroleum Systems and Earth History. Cambridge University Press.

Philp, R.P., Allen, J., Kuder, T., 2002. The use of the isotopic composition of individual compounds for correlating spilled oils and refined products in the environment with suspected sources. Environmental Forensics 3, 341–348.

Powell, T.G., McKirdy, D.M., 1973. Relationship between ratio of pristane to phytane, crude oil composition and geological environment. Nature Physical Science 243, 37–39.

Prince, R.C., Walters, C.C., 2007. Biodegradation of oil and its implications for source identification. In: Wang, Z., Stout, S.A. (Eds.), Oil Spill Environmental Forensics. Academic Press, Burlington, MA, pp. 349–379.

Rintoul, S.R., Hughes, C.W., Olbers, D., 2001. The Antarctic circumpolar current system. In: Ocean Circulation and Climate - Observing and Modeling the Global Ocean. International Geophysics 77, 271–302.

Ruble, T.E., Logan, G.A., Blevin, J.E., Struckmeyer, H.I.M., Ahmed, M., Quezada, R.A., 1999. Geochemistry of Palaeo-oil in Jerboa-1, Eyre Sub-basin, Great Australian Bight. CSIRO Petroleum Confidential Report No. 99-060, 223 p.

Radke, M., Welte, D.H., 1983. The methylphenanthrene index (MPI): a maturity parameter based on aromatic hydrocarbons. In: Bjoroy, M. et al. (Ed.), Advances in Organic Geochemistry 1981, Wiley, Chichester, pp. 504–512.

Ruble, T.E., Logan, G.A., Blevin, J.E., Struckmeyer, H.I.M., Liu, K., Ahmed, M., Eadington, P.J. and Quezada, R.A., 2001. Geochemistry and charge history of a palaeo-oil column: Jerboa-1, Eyre Sub-basin, Great Australian Bight. In: Hill, K.C., Bernecker T. (Eds.), Eastern Australasian Basins Symposium: A refocused energy perspective for the future. Petroleum Exploration Society of Australia, Special Publication, pp. 521–529.

Schmidt, T.C., Zwank, L., Elsner, M., Berg, M., Meckenstock, R.U., Haderlein, S.B., 2004. Compound-specific stable isotope analysis of organic contaminants in natural environments: a critical review of the state of the art, prospects, and future challenges. Analytical and Bioanalytical Chemistry 378, 283-300.

Schubotz, F., Lipp, J.S., Elvert, M., Kasten, S., Mollar P.X., Zabel, M., Bohrmann, G., Hinrichs, K., 2011. Petroleum degradation and associated microbial signatures at the Chapopote asphalt volcano, Southern Gulf of Mexico. Geochimica et Cosmochimica Acta 75, 4377–4398.

Seifert, W.K., Moldowan, J.M., 1979. The effect of biodegradation on steranes and terpanes in crude oils. Geochimica et Cosmochimica Acta 43, 111–126.

Smart, S.M., 1999. Asphaltites from the southern Australian Margin: Submarine oil seeps or maritime artifacts? BSc Honours thesis, National Centre for Petroleum Geology and Geophysics, University of Adelaide (unpublished).

Smith, M.A., Donaldson, I.F., 1995. The hydrocarbon potential of the Duntroon Basin. Australian Petroleum Exploration Association Journal, 35(1), 203–291.

Sofer, Z., 1984. Stable carbon isotope compositions of crude oils: application to source depositional environments and petroleum alteration. American Association of Petroleum Geologists Bulletin 68, 31-49.

Sprigg, R.C., 1986. A history of the search for commercial hydrocarbons in the Otway Basin complex. In: Glenie R.C. (Ed.), Second South-Eastern Australia Oil Exploration Symposium. Petroleum Exploration Society of Australia, Melbourne, pp. 173–200.

Sprigg, R.C., Woolley, J.B., 1963. Coastal bitumen in South Australia with special reference to observations at Geltwood Beach, south-eastern South Australia. Transactions of the Royal Society of South Australia 86, 67–103.

Struckmeyer, H.I.M., Totterdell, J.M., Blevin J.E., Logan, G.A., Boreham, C.J., Deighton, I., Krassay, A.A., Bradshaw, M.T., 2001. Character, maturity and distribution of potential Cretaceous oil source rocks in the Ceduna Sub-basin, Bight Basin, Great Australian Bight. In: Hill, K.C., Bernecker, T. (Eds.) Eastern Australasian Basins Symposium, A refocused energy perspective for the future, Melbourne, 2001. Petroleum Exploration Society of Australia. Special Publication, pp. 543–552.

Struckmeyer, H.I.M., Williams, A.K., Cowley, R., Totterdell, J.M., Lawrence, G., O'Brien, G.W., 2002. Evaluation of hydrocarbon seepage in the Great Australian Bight. Australian Petroleum Production and Exploration Association Journal 42(1), 371–385.

Summons, R.E., Fletcher, P. and Bradshaw, J., 1992. Hydrocarbon composition of stranded bitumen from the Northern territory. BMR Report and Professional Opinion.

Summons, R.E., Bradshaw, J., Burchardt, D.M., Goody, A.K., Murray, A.P., Foster, C.B., 1993. Hydrocarbon composition and origins of coastal bitumens from the Northern Territory, Australia. Petroleum Exploration Society of Australia Journal 21(1), 31–42.

Summons, R.E., Logan, G.A., Edwards, D.S., Boreham, C.J., Bradshaw, M.T., Blevin, J.E., Totterdell, J.M., Zumberge, J.E., 2001. Geochemical analogues for Australian coastal asphaltites - search for the source rock. Abstract. American Association of Petroleum Geologists Bulletin, 85 (Supplement).

Summons R.E., Powell T.G., 1986. Chlorobiaceae in Palaeozoic seas - Combined evidence from biological markers, isotopes and geology. Nature 319, 763–765.

Tolmer, A., 1882. Boat expedition to Kangaroo Island in pursuit of a gang of desperadoes, headed by Gilkes (in 1844). In: Reminiscences of an Adventurous and Chequered Career at Home and in the Antipodes. Sampson Low, Marston, Searle and Rivington, London, ch. 24.

Totterdell, J., Struckmeyer, H., 2003. Southern Australian Bight Basin holds deepwater potential. Offshore 63, 41–44.

Totterdell, J.M., Blevin, J.E., Struckmeyer, H.I.M., Bradshaw, B.E., Colwell, J.B., Kennard, J.M., 2000. A new sequence framework for the Great Australian Bight: Starting with a clean slate. Australian Petroleum, Production and Exploration Association Journal, 40, 95–117.

Totterdell, J.M., Struckmeyer, H.I.M., Boreham, C.J., Mitchell, C.H., Monteil, E. Bradshaw, B.E., 2008. Mid–Late Cretaceous organic-rich rocks from the Eastern Bight Basin: Implications for prospectivity. In: Blevin, J.E., Bradshaw, B.E., Uruski, C. (Eds.), Eastern Australasian Basins Symposium III, Petroleum Exploration Society Of Australia, Special Publication, pp. 137–158.

Volkman, J.K., Alexander, R., Kagi, R.I., Woodhouse, G.W., 1983. Demethylated hopanes in crude oils and their application in petroleum geochemistry. Geochimica et Cosmochimica Acta 47, 785-794.

Volkman, J.K., Alexander, R., Kagi, R.I., Rowland, S.J., Sheppard, P.N., 1984. Biodegradation of aromatic hydrocarbons in crude oils from the Barrow Sub-basin of Western Australia. Organic Geochemistry 6, 619–632.

Volkman J.K., O'Leary T., Summons R.E., Bendall M.R., 1992. Biomarker composition of some asphaltic coastal bitumens from Tasmania, Australia. Organic Geochemistry 18, 669–682.

Wade, A., 1915. Report on petroleum prospects in parts of western Victoria, South Australia and Western Australia. Government Printer, Melbourne. pp. 1–3. Extract from the archives of the Museum of South Australia, original source unknown.

Wakeham, S.G., Pease, T.K., 1992: Lipid analyses in marine particle and sediment samples: a laboratory handbook. Unpublished manuscript, Skidaway Institute of Oceanography, Savannah, Georgia, U.S.A.

Wardlaw, G.D., Arey, J.S., Reddy, C.M., Nelson, R.K., Ventura, G.T., Valentine, D.L., 2008. Disentangling oil weathering at a marine seep using GCxGC: broad metabolic specificity accompanies subsurface petroleum biodegradation. Environmental Science & Technology 42, 7166–7173.

Wardlaw, G.D., Nelson, R.K., Reddy, C.M., Valentine, D.L., 2011. Biodegradation preference for isomers of alkylated naphthalenes and benzothiophenes in marine sediment contaminated with crude oil. Organic Geochemistry 42, 630-639.

Wardroper, A.M.K., Hoffman, C.F., Maxwell, J.R., Barwise, A.J.G., Goodwin, N.S., Park, P.J.D., 1984 Crude oil biodegradation under simulated and natural conditions -II. Aromatic

steroid hydrocarbons. In: Schenck, P.A., de Leeuw, J.W., Lijmbach, G.W.M. (Eds.),

Advances in Organic Geochemistry 1983. Pergamon Press, Oxford, pp. 605–617.

Wenger, L.M., Davis, C.L., Isaksen, G.H., 2001. Multiple controls on petroleum

biodegradation and impact in oil quality. Society of Petroleum Engineers Reservoir

Evaluation and Engineering 5, 375–383.

Wenger, L.M., Isaksen, G.H., 2002. Control of hydrocarbon seepage intensity on level of

biodegradation in sea bottom sediments. Organic Geochemistry 33, 1277–1292.

Wilhelms, A., Larter, S.R., 1994a. Origin of tar mats in petroleum reservoirs. Part I:

Introduction and case studies. Marine and Petroleum Geology 11, 418–441.

Wilhelms, A., Larter, S.R., 1994b. Origin of tar mats in petroleum reservoirs. Part II:

Formation mechanisms for tar mats. Marine and Petroleum Geology 11, 442–456.

Wilhelms, A., Carpentier, B., Huc, A.Y., 1994. New methods to detect tar mats in petroleum

reservoirs. Journal of Petroleum Science and Engineering 12, 147–155.

Williams, J.A., Bjorøy, M., Dolcater, D.L., Winters, J.C., 1986. Biodegradation in South

Texas Eocene oils - effects on aromatics and biomarkers. Organic Geochemistry 10, 451-461.

7. Table and figure captions

Table 1 Sample identification, size and weight, location of stranding, year of collection and weathering description.

Sample	Location	Year	Dimensions L:W:D (mm)	Weight (g)	Degree of Weathering
CL1	Streaky Bay, Eyre Peninsula, SA	2005	138:94:37		Heavy
MH1	Frenchman's Rocks, Eyre Peninsula, SA	2005	83:71:26		Mild
80	Ravine des Casoars, Kangaroo Island, SA	1990	165:100:48	634	Moderate/Heavy
85	Seal Bay, Kangaroo Island, SA	1990		764	Moderate/Heavy
168	West Bay, Kangaroo Island, SA	1990		1944	Mild/Moderate
177	Bales Bay, Kangaroo Island, SA	1991	750:350:40	7000	Mild/Moderate
27A	Pether Rock, Canunda N.P., SA	1990	109:85:60	419	Mild
CB 32	Nine Mile Sandhill, Beachport, SA	1983	127:112:49		Moderate
162	German Point, Beachport, SA	1991	328:204:102	2876	Mild
NZ1	Invercargill, New Zealand	2002	273:256:87		Moderate
NZ2	Invercargill, New Zealand	2002	116:67:62		Moderate

Table 2 Selected bulk and biomarker parameters of the interior portion of the asphaltite specimens, including their relative standard deviation. See Appendix for peak abbreviations.

	Eyre Peninsula		Kangaroo Island				Limestone Coast			New Zealand		Average	% RSD
	CL1	MH1	80	85	168	177	27A	CB-32	162	NZ1	NZ2		
Bulk Composition (fullscan)													
Sats (%)	24.5	21.6	25.6	21.6	24.4	20.4	21.4	19.0	20.0	24.6	23.3	22.3	10%
Aroms (%)	15.2	12.0	16.2	12.7	13.6	11.4	14.1	16.4	13.3	13.1	12.7	13.7	12%
NSO (%)	18.6	16.5	10.4	14.7	16.3	15.6	16.7	15.9	14.2	16.9	19.4	15.6	15%
Asph (%)	41.7	49.9	47.8	51.0	45.7	52.6	47.8	48.7	52.5	45.4	44.6	48.5	7%
Normal & Acyclic Hydrocarbons (fullscan)													
Pr/Ph	1.18	1.12	1.11	1.07	1.14	1.10	1.12	1.06	1.10	1.10	1.14	1.11	3%
Pr/nC_{17}	0.47	0.49	0.48	0.58	0.48	0.47	0.50	0.56	0.51	0.47	0.48	0.50	8%
Ph/nC_{18}	0.41	0.44	0.41	0.52	0.41	0.40	0.46	0.48	0.46	0.44	0.43	0.45	8%
OEP	1.04	1.04	1.04	1.02	1.02	1.03	1.02	1.02	1.02	1.04	1.03	1.03	1%
Terpanes (m/z 191)													
$C_{29}BNH/C_{30}H$	0.05	0.06	0.06	0.06	0.06	0.06	0.05	0.06	0.06	0.07	0.05	0.06	8%
$C_{29}H/C_{30}H$	0.67	0.70	0.65	0.70	0.72	0.70	0.71	0.66	0.71	0.75	0.60	0.69	6%
$C_{30}DiaH/C_{30}H$	0.08	0.07	0.09	0.09	0.08	0.09	0.09	0.09	0.09	0.07	0.10	0.09	10%
$C_{30}Ts/C_{30}H$	0.09	0.08	0.09	0.09	0.09	0.09	0.09	0.09	0.09	0.08	0.09	0.09	6%
$Gam/C_{31}HR$	0.17	0.17	0.17	0.17	0.17	0.17	0.15	0.17	0.18	0.18	0.18	0.17	4%
Ts/(Ts+Tm)	0.37	0.38	0.39	0.39	0.38	0.39	0.40	0.38	0.38	0.40	0.39	0.39	2%
$C_{29}Ts/(C_{29}Ts+C_{29}H)$	0.22	0.22	0.24	0.22	0.21	0.23	0.22	0.24	0.22	0.20	0.26	0.23	8%
$Mor/C_{30}H$	0.13	0.12	0.13	0.13	0.13	0.13	0.12	0.13	0.13	0.12	0.13	0.13	4%
C_{32} S/(S+R)	0.58	0.59	0.60	0.59	0.59	0.60	0.59	0.60	0.60	0.59	0.60	0.60	1%
C_{35} Homohopane Index	0.07	0.06	0.06	0.06	0.06	0.05	0.06	0.05	0.06	0.06	0.07	0.06	9%
$C_{35}(S+R)/C_{31}(S+R)$	0.15	0.14	0.12	0.12	0.11	0.12	0.12	0.10	0.13	0.12	0.15	0.12	12%
C_{35}/C_{34} (S only)	0.66	0.66	0.69	0.69	0.73	0.72	0.59	0.61	0.77	0.53	0.60	0.66	11%
Steranes (m/z 217)													
% C_{27} ααα 20R	33.7	36.7	38.5	35.0	38.0	38.7	35.2	37.3	38.2	36.7	36.7	37.1	4%
% C_{28} ααα 20R	23.3	23.3	23.8	25.0	23.3	25.1	24.5	23.9	24.1	24.3	22.3	24.0	3%
% C_{29} ααα 20R	43.0	40.1	37.7	40.1	38.7	36.3	40.3	38.9	37.6	39.1	40.9	38.8	5%
C_{27} Dia/(Dia+Reg)	0.48	0.52	0.48	0.53	0.53	0.48	0.51	0.48	0.49	0.48	0.55	0.50	5%
C_{29} αββ/(ααα+αββ)	0.51	0.52	0.48	0.51	0.52	0.51	0.50	0.50	0.51	0.52	0.51	0.51	2%
αββ−Steranes (m/z 218)													
% C_{27} αββ 20(R+S)	35.7	37.6	39.3	38.0	38.4	38.4	37.7	37.8	38.6	38.9	37.0	38.2	3%
% C_{28} αββ 20(R+S)	27.6	27.8	27.8	27.7	27.5	27.4	28.1	27.7	27.3	28.0	28.3	27.8	1%
% C_{29} αββ 20(R+S)	36.7	34.6	32.9	34.3	34.1	34.2	34.2	34.5	34.1	33.1	34.7	34.0	3%
C_{29}/C_{27} αββ Sterane Ratio	1.03	0.92	0.84	0.90	0.89	0.89	0.91	0.91	0.88	0.85	0.94	0.89	6%
Tricyclic/Pentacyclic Terpanes	0.10	0.15	0.14	0.15	0.16	0.16	0.17	0.14	0.16	0.18	0.13	0.16	15%
Steranes/Terpanes	0.37	0.43	0.42	0.44	0.47	0.46	0.46	0.43	0.44	0.51	0.38	0.45	9%
% Tricyclic Terpanes	6.62	8.99	8.52	9.16	9.61	9.44	10.0	8.73	9.33	10.2	8.30	9.26	11%
% Pentacyclic Terpanes	66.1	61.2	61.8	60.2	58.3	59.2	58.5	61.2	59.9	55.8	64.1	59.9	5%
% Steranes	27.2	29.8	29.7	30.6	32.1	31.4	31.5	30.0	30.8	34.0	27.7	30.9	6%
Triaromatic Steroids (m/z 231)													
% C_{26} Triaromatic Steroids	21.9	18.5	19.2	19.9	18.8	19.2	19.6	19.7	20.1	20.7	19.3	19.7	5%
% C_{27} Triaromatic Steroids	39.6	42.5	42.4	42.2	42.0	41.7	40.9	41.5	41.1	44.4	41.5	41.8	3%
% C_{28} Triaromatic Steroids	32.0	32.7	32.5	32.0	32.8	33.2	32.6	32.3	32.5	28.2	32.2	32.1	4%
% C_{29} Triaromatic Steroids	6.6	6.4	6.0	6.0	6.3	5.9	6.9	6.4	6.3	6.7	7.0	6.4	6%
Polycyclic Aromatic Hydrocarbons & Thiophenes (m/z 178, 184, 198, 226, 252)													
BaP/BbF	2.24	2.18	1.83	1.70	2.02	1.98	2.05	1.97	1.79	1.86	1.82	1.89	9%
P/MP	0.47	0.50	0.46	0.44	0.42	0.52	0.41	0.38	0.41	0.44	0.44	0.44	9%
P/C2P	0.47	0.50	0.40	0.40	0.38	0.52	0.29	0.34	0.38	0.43	0.42	0.40	16%
DBT/MDBT	0.42	0.56	0.44	0.15	0.40	0.53	0.54	0.24	0.30	0.44	0.39	0.38	32%
DBT/C3DBT	0.28	0.46	0.23	0.02	0.26	0.44	0.43	0.11	0.17	0.33	0.29	0.25	51%
Aromatic Maturity Indices (m/z 178,192)													
MPI-1	0.60	0.61	0.62	0.62	0.64	0.60	0.66	0.65	0.63	0.63	0.64	0.63	3%
MPR	0.68	0.68	0.66	0.65	0.67	0.67	0.66	0.68	0.65	0.66	0.66	0.66	2%
Rc (%)	0.76	0.77	0.77	0.77	0.78	0.76	0.80	0.79	0.78	0.78	0.79	0.78	1%

Table 3 Percentage difference in selected bulk and molecular parameters between the inner and outer portions of asphaltite specimens. See Appendix for peak abbreviations.

	Eyre Peninsula		Kangaroo Island				Limestone Coast			New Zealand	
	CL1	MH1	80	85	168	177	27A	CB-32	162	NZ1	NZ2
Bulk Composition						Difference inner – outer (%)					
Sats (%)	-33.3	-18.7	-31.7	0.9	-14.5	-6.1	-9.8	-15.3	-8.9	-18.7	-16.7
Aroms (%)	-30.3	12.5	-32.3	-6.5	-23.0	8.4	-5.1	-31.0	-12.0	-3.9	0.8
NSO (%)	-14.4	3.0	44.2	7.8	-21.8	4.4	1.2	20.8	17.4	26.2	6.5
Asph (%)	27.9	3.2	11.1	-1.2	18.5	-1.0	5.1	6.7	0.9	-0.9	4.8
Normal Hydrocarbons (fullscan)											
C_{10-19}/C_{30}	7.1	8.1	5.0	11.8	2.1	20.7	16.3	38.7	27.8	5.7	7.6
Terpanes (*m/z* 191)											
C_{35} Homohopane Index	-40.7	-37.8	-29.4	-23.7	-30.5	-27.2	-19.2	-5.4	-28.3	-23.1	-38.2
$C_{35}(S+R)/C_{31}(S+R)$	-50.7	-45.7	-36.3	-28.4	-23.8	-32.5	-24.4	-11.5	-33.6	-28.0	-46.8
Steranes (*m/z* 217)											
% C_{27} ααα 20R	16.9	3.9	-0.1	14.2	5.5	-0.6	7.5	12.3	-3.9	9.9	17.6
% C_{28} ααα 20R	-7.0	-6.9	-1.3	0.1	4.9	-9.7	-9.5	-9.1	1.0	-5.9	0.1
% C_{29} ααα 20R	-11.4	0.2	1.0	-14.3	-8.9	6.8	-1.3	-7.5	3.2	-6.4	-19.0
αββ– Steranes (*m/z* 218)											
% C_{27} αββ 20(R+S)	8.6	6.8	0.3	3.2	2.9	4.6	3.9	3.3	-0.2	0.8	11.4
% C_{28} αββ 20(R+S)	1.8	-7.3	-0.4	-3.1	-1.7	3.4	-1.9	-0.6	-2.7	-0.7	-4.1
% C_{29} αββ 20(R+S)	-10.6	-2.1	0.0	-1.2	-2.0	-8.3	-2.8	-3.2	2.3	-0.3	-10.1
C29 ααα 20S/20R	21.6	6.7	-6.2	8.2	-6.7	-16.8	9.9	26.6	-9.6	3.5	35.9
C_{29}/C_{27} αββ Sterane Ratio	-19.1	-8.9	-0.3	-4.4	-4.9	-12.9	-6.7	-6.5	2.5	-1.1	-21.5
Tricyclic/Pentacyclic Terpanes	59.4	30.5	37.5	21.0	17.4	29.8	12.4	19.3	20.4	0.4	32.5
Steranes/Terpanes	30.6	18.2	19.6	11.4	5.1	17.3	9.1	13.2	9.3	-3.6	24.2
% Tricyclic Terpanes	43.7	20.3	26.1	14.4	13.1	19.5	7.6	12.6	14.5	1.6	21.0
% Pentacyclic Terpanes	-16.7	-10.3	-11.7	-6.7	-4.3	-10.5	-4.9	-6.8	-6.0	1.1	-11.7
% Steranes	21.4	12.4	13.4	7.8	3.4	11.6	6.2	9.0	6.3	-2.4	16.9
Triaromatic Steroids (*m/z* 231)											
% C_{26} Triaromatic Steroids	-4.1	-0.1	-0.1	-1.5	0.2	-0.2	-1.0	-0.5	-1.8	-3.3	-0.7
% C_{27} Triaromatic Steroids	3.6	0.7	0.3	1.0	0.1	1.1	2.0	0.7	1.3	-0.7	1.3
% C_{28} Triaromatic Steroids	0.3	-0.4	-0.4	-0.1	-0.1	-1.0	-0.9	-0.1	0.2	4.2	0.2
% C_{29} Triaromatic Steroids	0.2	-0.3	0.3	0.6	-0.2	0.1	-0.1	-0.1	0.3	-0.1	-0.8
Polycyclic Aromatic Hydrocarbons & Thiophenes (*m/z* 178, 184, 198, 226, 252)											
BaP/BbF	-15.4	-2.4	-5.0	-1.3	-2.0	-0.4	-0.5	-4.3	-0.1	-3.0	-4.7
P/MP	-10.4	0.4	1.0	-1.2	-3.8	-1.3	-1.9	-12.3	-6.7	63.1	-10.3
P/C2P	-12.2	-1.9	-4.4	-1.5	-6.7	-2.0	2.3	-18.8	-6.0	90.5	-12.9
DBT/MDBT	-3.0	19.7	33.0	-47.9	-12.3	-9.9	12.2	-51.7	-8.1	-36.1	-32.4
DBT/C3DBT	-2.8	12.0	9.0	-10.7	-7.2	-6.0	0.8	-17.2	-0.3	12.1	-18.4

Table 4 Carbon isotopic compositions of individual *n*-alkanes in the outer and inner portions of the asphaltite specimens

n-alkane carbon number	Eyre Peninsula						Kangaroo Island											
	CL1			MH1			80			85			168			177		
	outer (‰)	inner (‰)	diff (‰)	outer (‰)	inner (‰)	diff (‰)	outer (‰)	inner (‰)	diff (‰)	outer (‰)	inner (‰)	diff (‰)	outer (‰)	inner (‰)	diff (‰)	outer (‰)	inner (‰)	diff (‰)
15	-34.7	-34.5	-0.2	-34.7	-34	-0.7	-34.8	-36	1.3	-35.3	-35.8	0.4	-34.7	-34.3	-0.4	-34.7	-34.9	0.2
16	-34.6	-34	-0.5	-34.5	-33.5	-1	-34.3	-35.5	1.3	-34.9	-35.3	0.4	-34.4	-34.2	-0.2	-33.9	-34.3	0.4
17	-34.7	-33.9	-0.8	-34.4	-33.3	-1.1	-34.1	-35.7	1.6	-34.7	-35.2	0.5	-34.3	-34.3	0	-33.5	-34.1	0.6
18	-35	-34.1	-0.9	-34.5	-33.4	-1.1	-34.1	-35.7	1.6	-34.7	-35.2	0.5	-34.2	-34.4	0.2	-33.4	-34.2	0.9
19	-35.4	-34.3	-1.1	-34.7	-33.5	-1.2	-34.2	-36.1	1.9	-34.8	-35.5	0.6	-34.4	-34.8	0.4	-33.7	-34.4	0.8
20	-35.6	-34.4	-1.2	-34.9	-33.7	-1.1	-34.4	-36.2	1.8	-35	-35.5	0.6	-34.5	-35	0.5	-33.4	-34.6	1.2
21	-35.9	-34.8	-1.1	-35.2	-34	-1.3	-34.5	-36.4	1.8	-35.3	-35.9	0.6	-34.7	-35.2	0.5	-33.7	-34.8	1.1
22	-36.3	-34.9	-1.4	-35.3	-33.9	-1.4	-34.6	-36.3	1.7	-34.9	-35.8	0.9	-34.8	-35.3	0.5	-33.8	-34.9	1.1
23	-36.4	-35.1	-1.3	-35.5	-34.2	-1.3	-34.8	-36.7	1.9	-35.3	-36	0.7	-35	-35.7	0.7	-33.6	-34.9	1.3
24	-36.2	-34.9	-1.3	-36	-34	-2	-34.5	-36.1	1.6	-34.9	-35.9	1	-34.8	-35.5	0.7	-34	-35	1
25	-36.9	-35.5	-1.5	-36.1	-34.6	-1.5	-35.1	-36.7	1.5	-35.3	-36.4	1.2	-35.2	-36.4	1.2	-33.7	-35.2	1.5
26		-35.1		-36	-34.2	-1.9	-34.9	-36.1	1.4	-34.9	-35.7	1	-34.8	-35.7	0.9	-33.9	-34.9	1
27		-35.1		-36	-34.4	-1.7	-34.8	-36.6	1.7	-35	-35.9	0.9	-35	-36	0.9	-33.6	-34.9	1.3
28					-34.1		-34.7			-34.8	-35.8	1	-34.8	-35.8	1	-33.7	-35.1	1.3
29							-35.5			-35	-36.1	1.1				-33.3	-35.1	1.8
30							-35						-34.8			-34.3	-35.3	1
31										-35.2								

| n-alkane carbon number	Limestone Coast									New Zealand					
	27A			CB-32			162			NZ1			NZ2		
	outer (‰)	inner (‰)	diff (‰)	outer (‰)	inner (‰)	diff (‰)	outer (‰)	inner (‰)	diff (‰)	outer (‰)	inner (‰)	diff (‰)	outer (‰)	inner (‰)	diff (‰)
15	-35.4	-35.5	0.2				-34.3	-33.7	-0.6	-35.8	-34.5	-1.3		-34.4	
16	-35	-35	0	-36.6			-34.3	-33.3	-1	-35.3	-34	-1.3	-35.2	-34	-1.2
17	-35	-35.1	0.2	-36.2	-34.7	-1.5	-34.1	-33.4	-0.8	-35.1	-34	-1.2	-35.2	-34.1	-1.1
18	-35.1	-35.5	0.4	-36	-35.2	-0.8	-34.1	-33.3	-0.8	-35.2	-34	-1.2	-35.5	-34.2	-1.3
19	-35.2	-35.4	0.1	-36	-35.4	-0.5	-34.2	-33.7	-0.6	-35.4	-34.1	-1.3	-35.6	-34.4	-1.2
20	-35.4	-35.7	0.3	-36.1	-35.5	-0.6	-34.3	-33.9	-0.5	-35.6	-34.3	-1.3	-35.6	-34.6	-1
21	-35.6	-35.8	0.3	-36.4	-35.9	-0.4	-34.6	-34.1	-0.5	-35.9	-34.5	-1.4	-36	-34.8	-1.2
22	-35.5	-35.9	0.4	-36.4	-36	-0.4	-34.4	-34.1	-0.3	-36	-34.6	-1.4	-36.1	-34.9	-1.1
23	-35.9	-36	0.1	-36.6	-36	-0.6	-34.9	-34.3	-0.6	-36.3	-34.9	-1.4	-35.9	-35	-0.9
24	-35.6	-36.1	0.4	-36.2	-35.7	-0.5	-34.3	-34.2	-0.1	-35.9	-34.7	-1.3	-36.2	-35	-1.2
25	-36	-36.2	0.3	-36.8	-36.5	-0.3	-34.9	-34.6	-0.2	-36.5	-35.3	-1.2	-36.4	-35.1	-1.2
26	-35.4	-36.3	0.8	-36.4	-35.7	-0.7	-34.1	-34.1	0.1	-36.2	-34.8	-1.4		-35.1	
27	-35.5	-36.2	0.6	-36.4	-36.3	-0.1	-34.6	-34.3	-0.2	-36.2	-35	-1.2		-35.1	
28	-35.9	-35.9	0.1	-36.2	-35.5	-0.8	-34.3	-34.1	-0.2	-36	-34.8	-1.3		-35	
29	-35.7			-36.4	-35.2	-1.1	-34.9	-34.9	0	-36.2	-35.6	-0.7		-35.1	
30	-36			-36.2			-34.1	-34.4	0.3	-36.1	-34.9	-1.1		-35.1	
31															
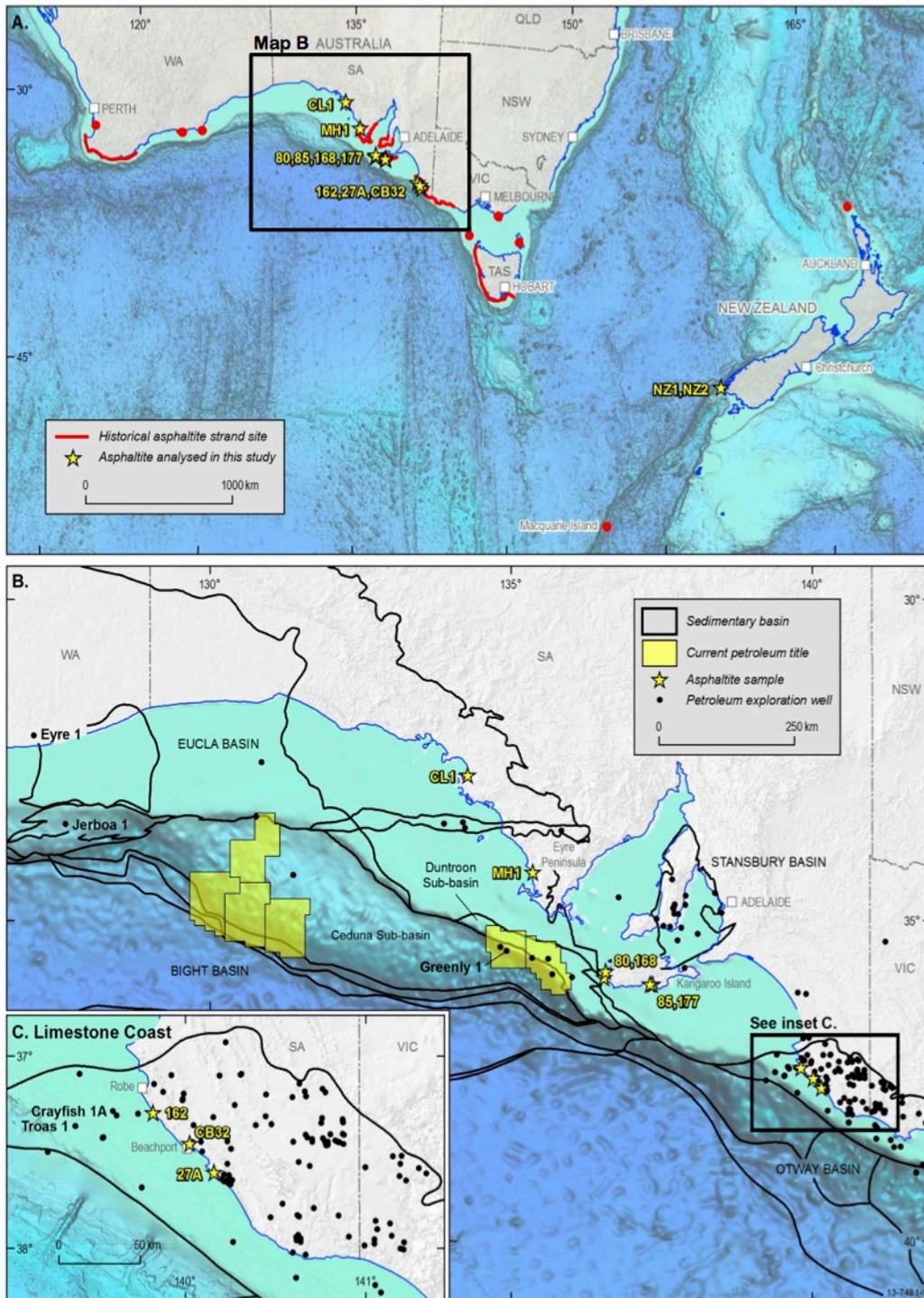
Fig. 1 A) location of historically documented asphaltite strandings and samples from this study; B) expanded section for South Australia with sample stranding sites, basin locations and petroleum exploration well sites; C) expanded section for the Limestone Coast, South Australia with sample stranding sites and petroleum exploration well sites.
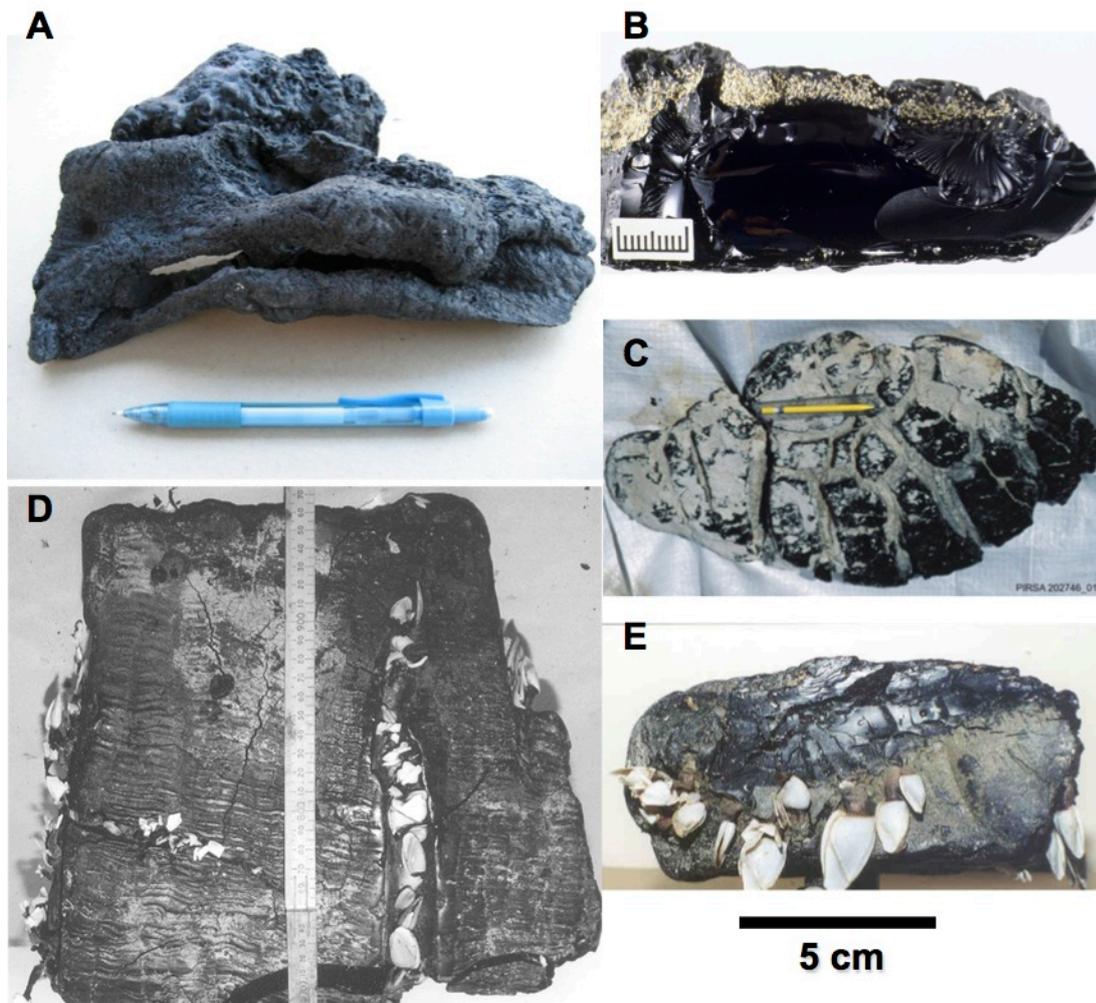
Fig. 2 Examples of asphaltite strandings: A) an asphaltite from Port McDonnell (not analysed) with a rolled over edge indicative of viscous flow; B) sample 80, Ravine de Casours, Kangaroo Island, broken open to reveal the conchoidal fracture pattern typical of all asphaltites (scale bar 20 mm); C) sample 177, Bales Bay, Kangaroo Island, a large specimen exhibiting upper surface devolatilization cracks and a characteristic flat ovoid shape (long axis = 75 cm); D) sample NZ1, Invercargill, New Zealand with an unusual internal fabric suggestive of laminar flow, devolatilization cracks and a bivalve colony; E) sample NZ2, Invercargill, New Zealand, also colonised by bivalves. Photographs provided by D. McKirdy (plate A); D. Edwards, nee Padley (plates B and C); and D. Bradley (plates D and E).
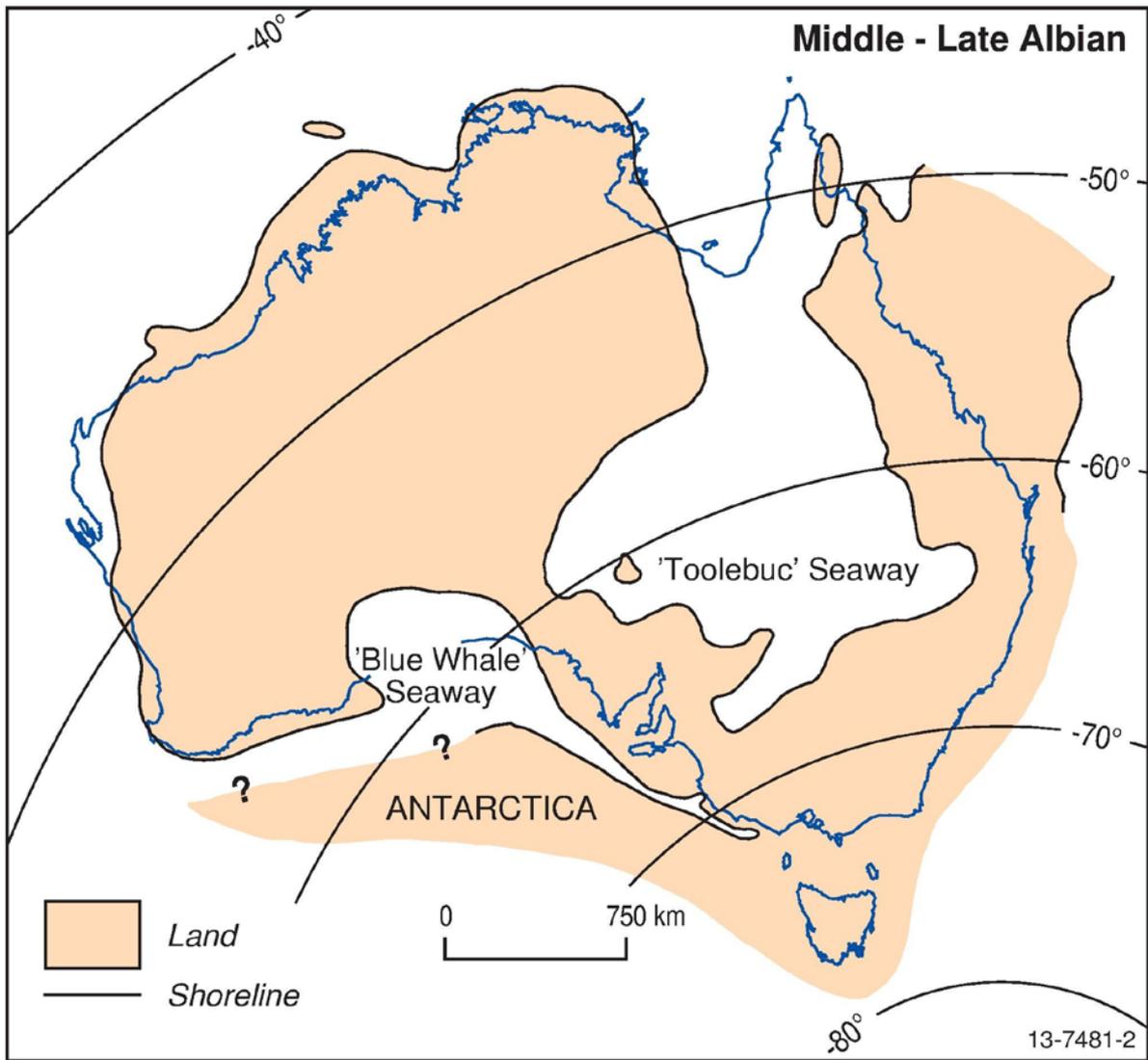
Fig. 3 Middle to late Albian palaeogeography of Australia showing the location of the Blue Whale and Toolebuc seaways (after Boreham et al., 2001).
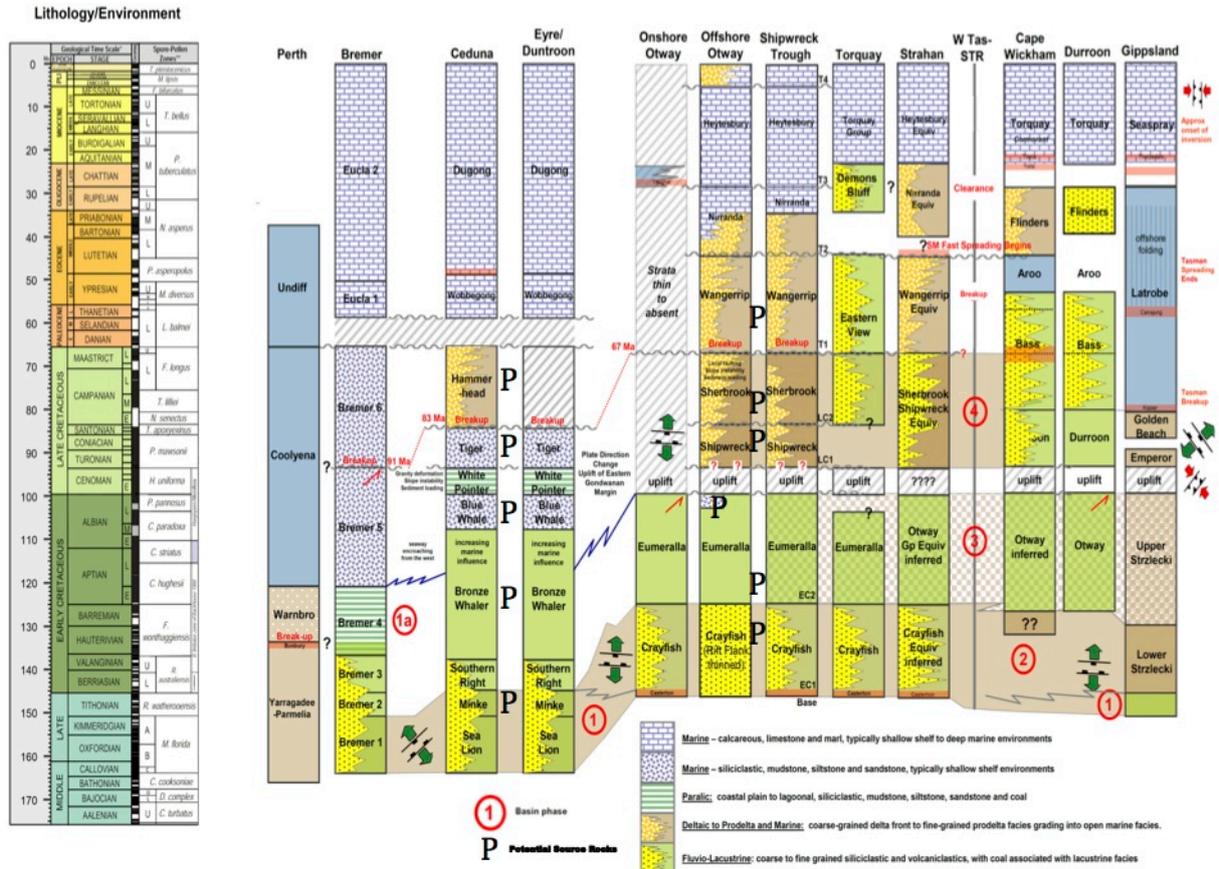
Fig. 4 Stratigraphy of the southern margin basins (after Blevin and Cathro, 2008). Basin phases: 1) mechanical extension; 2) thermal subsidence-1; 3) accelerated subsidence; 4) thermal subsidence-2.
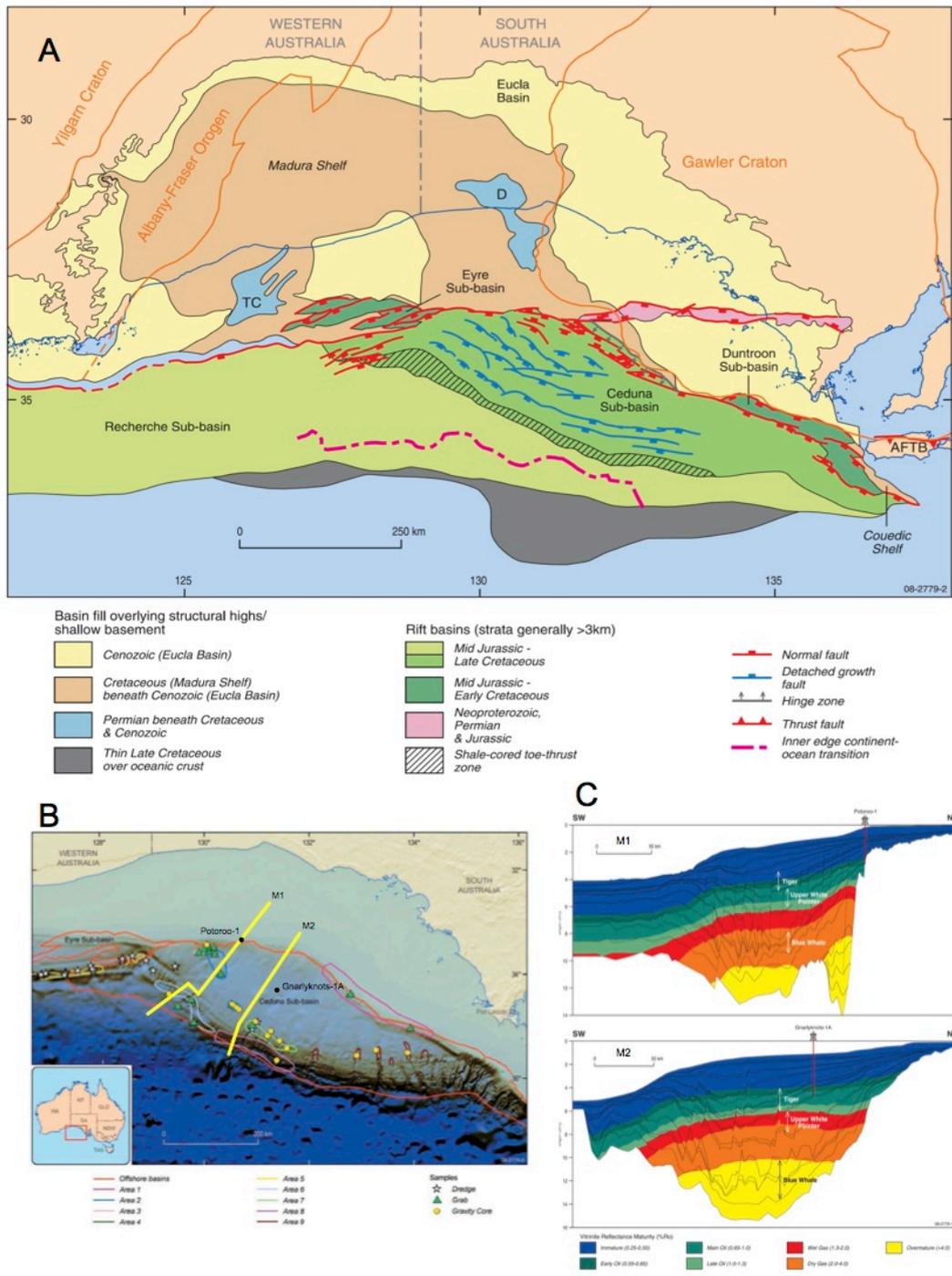
Fig. 5 A) Structural elements map of the eastern Bight Basin (note: the Bremer and Denmark sub-basins lie to the west of the Recherche Sub-basin); B) Survey areas and location of sampling sites in Geoscience Australia's Bight Basin Sampling and Seepage Survey SS01/2007; C) Modelled present-day maturity zones (% R_o) for the transects marked in yellow on map B (all after Totterdell et al., 2008).
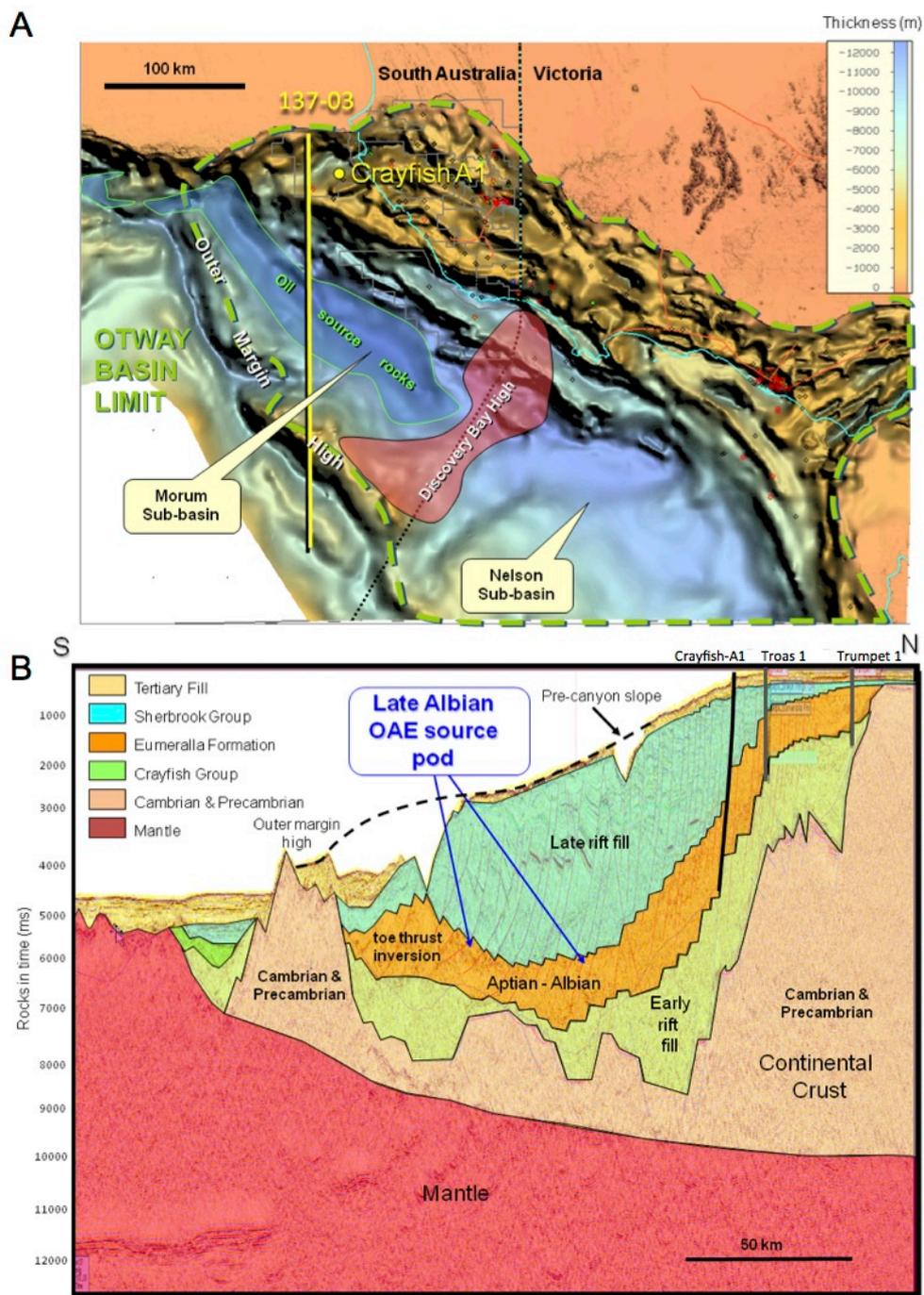
Fig. 6 A) Outline of Otway Basin with inferred sediment thickness and sub-basin, seismic section 137-03 and Crayfish-A1 well locations; and B) Interpretation of seismic section 137-03, showing the location of the possible upper Albian OAE source pod (after Boult et al., 2005).
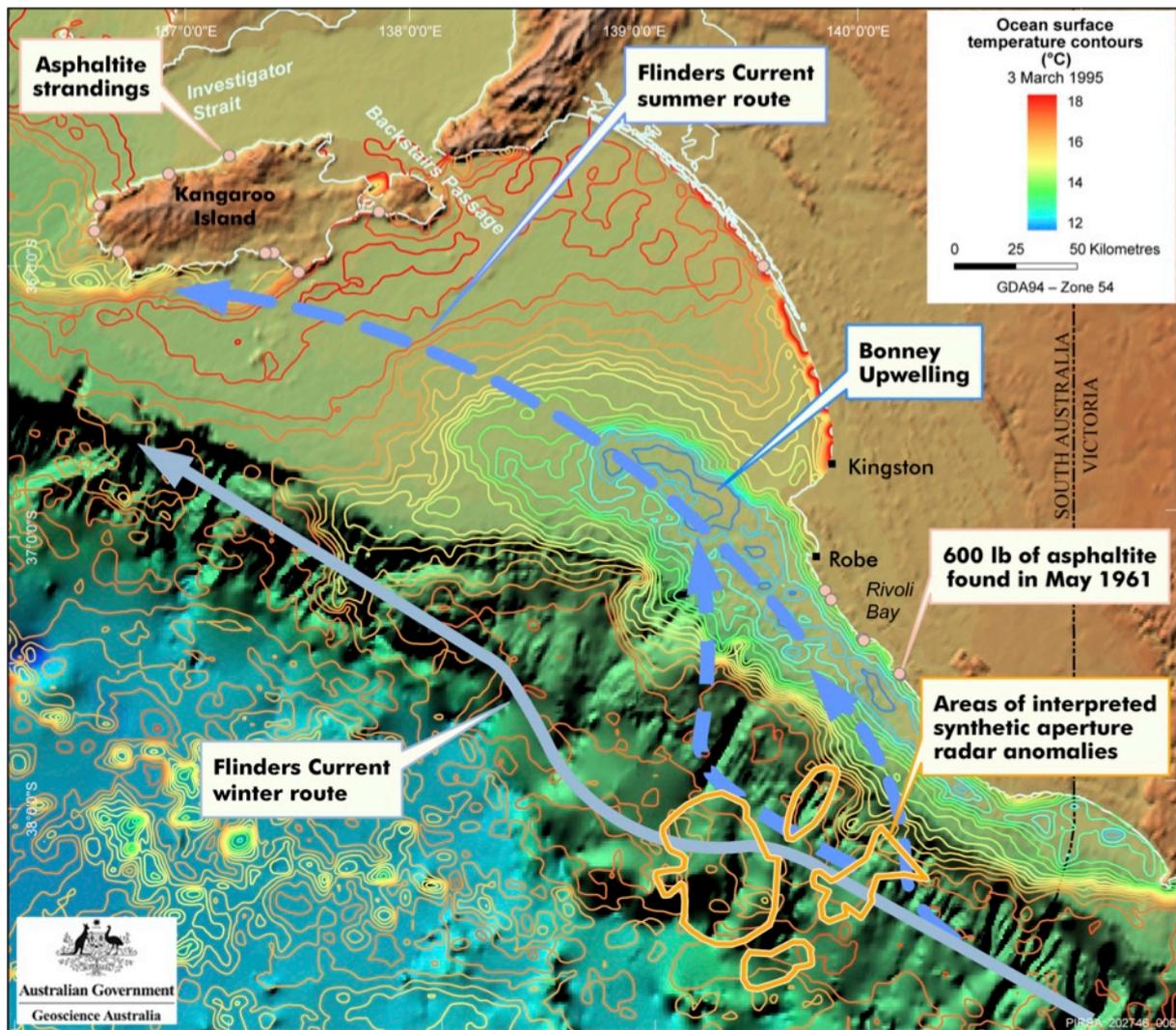
Fig. 7 Bathymetry of the South Australian continental margin with an overlay of surface temperature contours of 3rd March 1995, showing the location of the deep-water Flinders Current, Bonney Upwelling, asphaltite strandings and SAR anomalies (Boult et al., 2005).
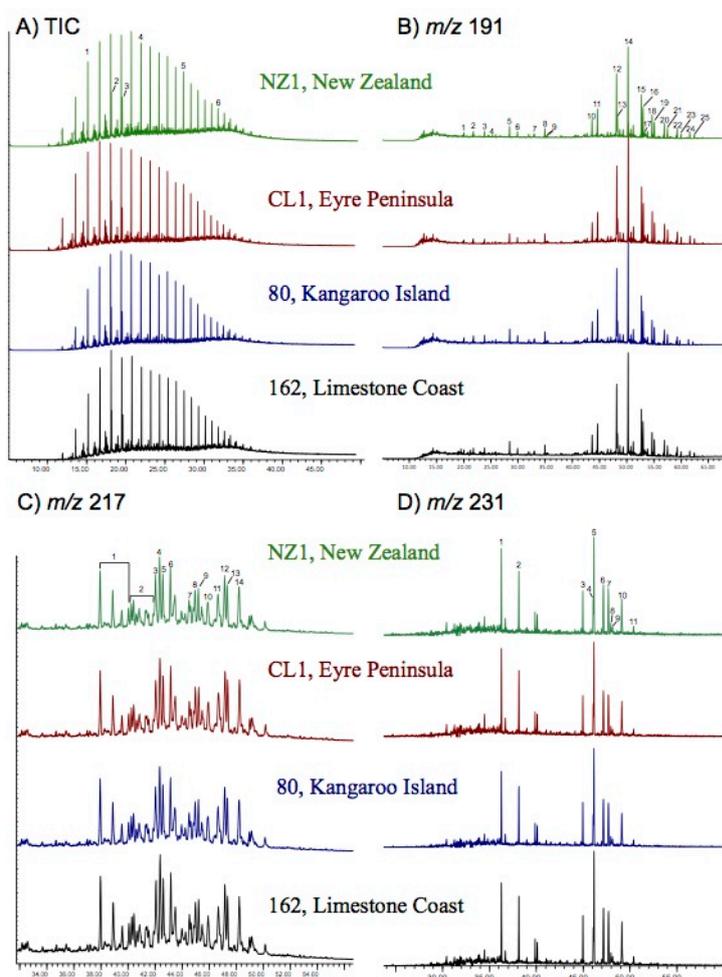
Fig. 8 Selected chromatograms of saturated and aromatic hydrocarbons in the interior portion of representative asphaltite specimens from each stranding domain: A) TIC of saturated hydrocarbon fraction [1, nC_{15}; 2, Pr; 3, Ph; 4, nC_{20}; 5, nC_{25}; 6, nC_{30}]; B) m/z 191, terpanes [1–7 & 9, C_{19}–C_{26}T; 8, Tet; 10, Ts; 11, Tm; 12, $C_{29}\alpha\beta$; 13, C_{29}Ts; 14, $C_{30}\alpha\beta$; 15, C_{31}HS; 16, C_{31}HR; 17, Gam; 18, C_{32}HS; 19, C_{32}HR; 20, C_{33}HS; 21, C_{33}HR; 22, C_{34}HS; 23, C_{34}HR; 24, C_{35}HS; 25, C_{35}HR]; C) m/z 217, steranes* [1, C_{27} diasteranes; 2, C_{28} diasteranes; 3, $C_{27}\alpha\alpha\alpha20S$; 4, $C_{27}\alpha\beta\beta20R$; 5, $C_{27}\alpha\beta\beta20S$; 6, $C_{27}\alpha\alpha\alpha20R$; 7, $C_{28}\alpha\alpha\alpha20S$; 8, $C_{28}\alpha\beta\beta20R$; 9, $C_{28}\alpha\beta\beta20S$; 10, $C_{28}\alpha\alpha\alpha20R$; 11, $C_{29}\alpha\alpha\alpha20S$; 12, $C_{29}\alpha\beta\beta20R$; 13, $C_{29}\alpha\beta\beta20S$; 14, $C_{29}\alpha\alpha\alpha20R$]; and D) m/z 231, triaromatic steroids [1, C_{20}; 2, C_{21}; 3, C_{26} 20S; 4, C_{26} 20R; 5, C_{27} 20S; 6, C_{28} 20S; 7, C_{27} 20R; 8, C_{29} 20S 9α; 9, C_{29} 20S 9β; 10, C_{28} 20R; 11, C_{29} 20R]. See Appendix for key to peak abbreviations. *Some co-elution of regular and diasterane isomers is noted.
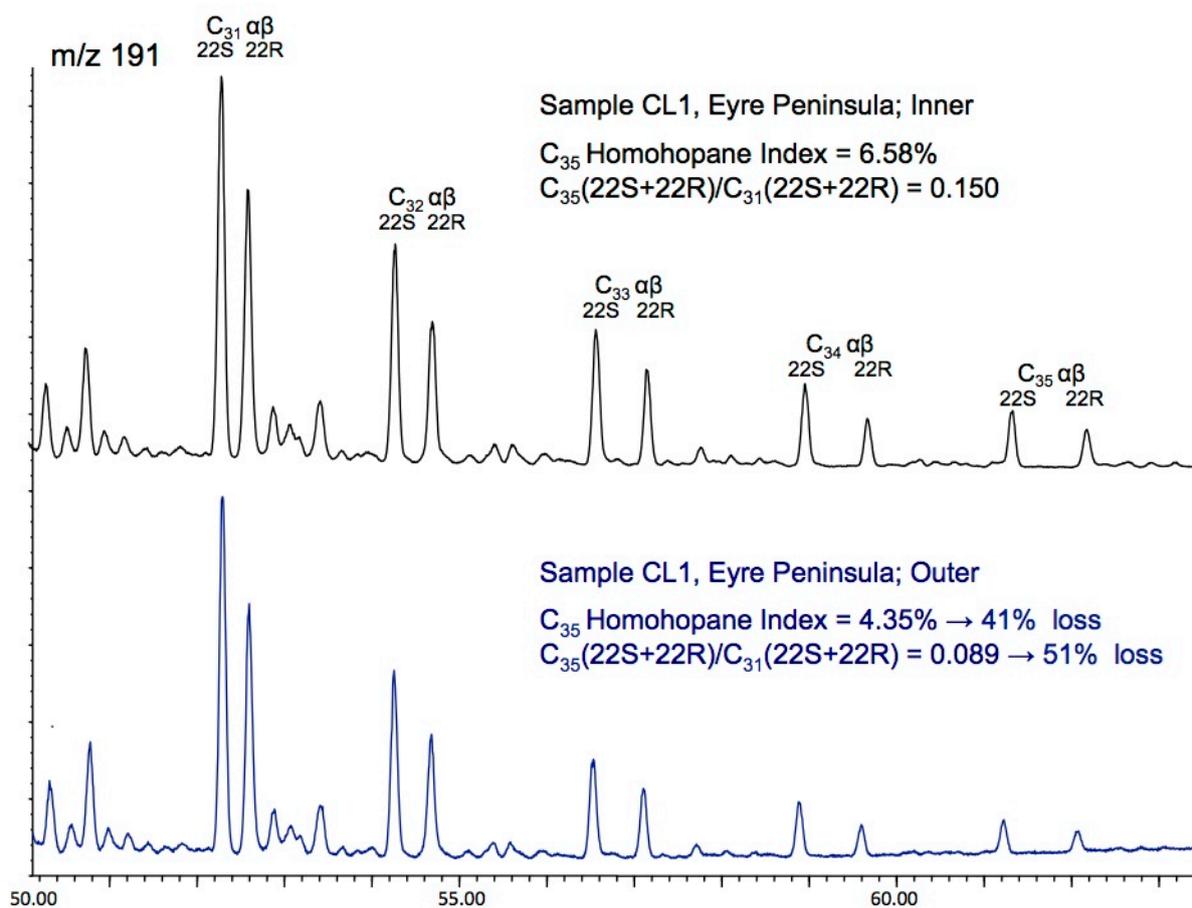
Fig. 9 Partial *m/z* 191 chromatograms of the inner and outer portions of sample CL1, Eyre Peninsula, expanded to highlight their C_{31}–C_{35} $17\alpha,21\beta(H)$ homohopane 22S & 22R distributions. See Appendix for key to peak abbreviations.
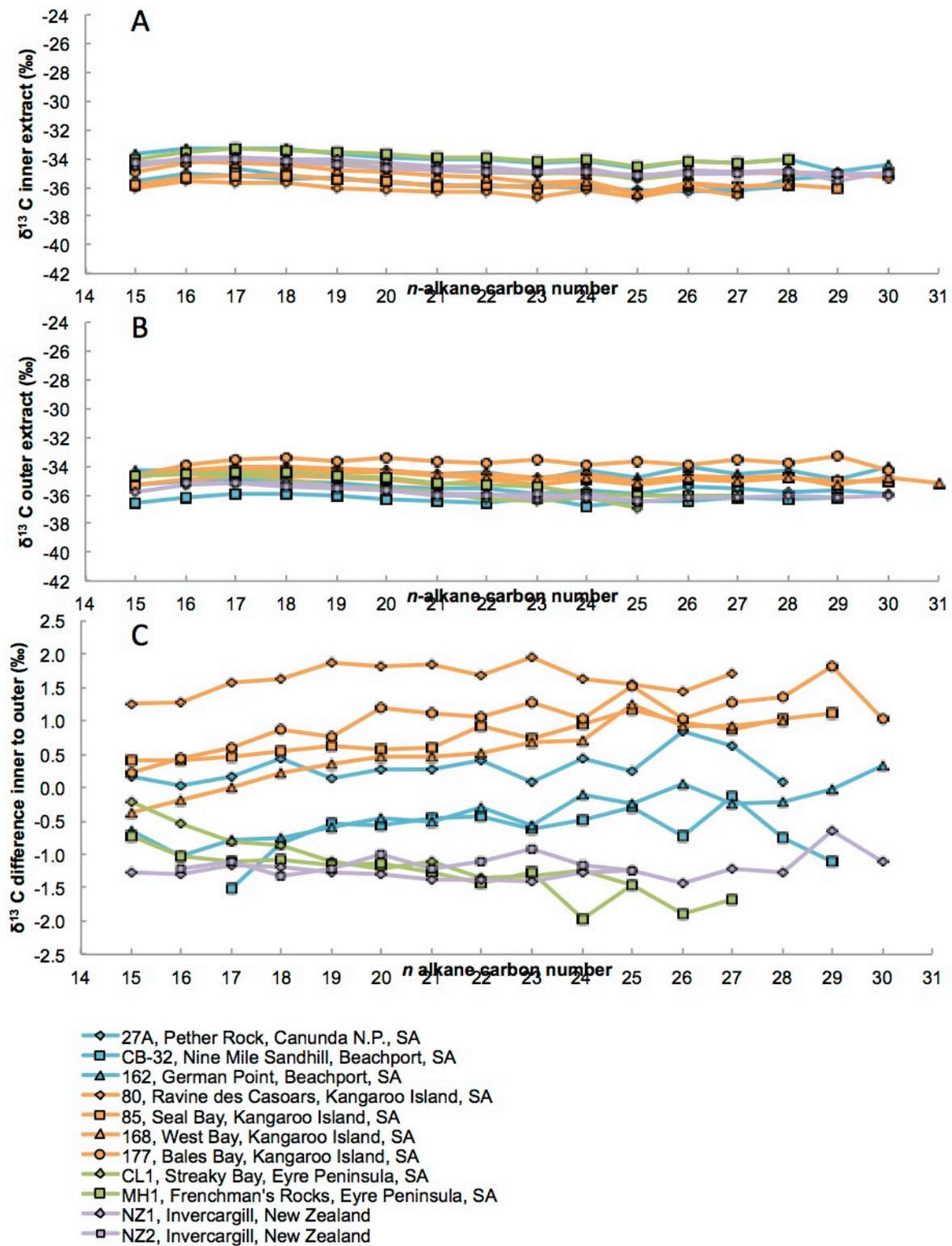
Fig. 10 Plots of *n*-alkane δ^{13}C versus carbon number for asphaltite specimens: A) inner

portion, B) outer portion and C) the difference between inner and outer.

Appendix

Abbreviations for Tables 2 & 3 and Figures 8 & 9:

Bulk Composition

Sats = Saturated hydrocarbons

Arom = Aromatic hydrocarbons

NSO = Polar compounds

Asph = Asphaltenes

Normal & Acyclic Hydrocarbons (fullscan)

nC$_x$ = normal alkane C$_{carbon\ number}$ e.g. nC$_{15}$ = n-pentadecane

Pr = pristane

Ph = phytane

C$_{10-19}$/C$_{30}$ = ($\sum n$C$_{10}$ – nC$_{19}$)/nC$_{30}$

OEP = odd/even predominance = (nC$_{21}$ + (6 x nC$_{23}$) + nC$_{25}$) / ((4 x nC$_{22}$) + (4 x nC$_{24}$))

Hopanes (*m/z* 191)

T = tricyclic terpanes. Note C$_{25}$ and C$_{26}$ homologues have a chiral centre at C$_{22}$ (R & S)

Tet = C$_{24}$ tetracyclic terpane

Ts = C$_{27}$ 18α(H)-22,29,30-trisnorneohopane

Tm = C$_{27}$ 17α(H)-22,29,30-trisnorhopane

C$_{28}$BNH = C$_{28}$ 17α(H),21β(H)-28,30 bisnorhopane

C$_{29}$H = C$_{29}$ 17α(H),21β(H)-hopane

C$_{30}$H = C$_{30}$ 17α(H),21β(H)-hopane

Mor = C$_{30}$ 17β(H),21α(H)-moretane

Normor = C$_{29}$ 17β(H),21α(H)-normoretane

C$_{30}$DiaH = C$_{30}$ 17α(H),21β(H)-diahopane

C$_{29}$Ts = C$_{29}$ 30-norneohopane

C$_{30}$Ts = C$_{30}$ 30-norneohopane

Gam = Gammacerane

C$_{31}$HS = C$_{31}$ 17α(H),21β(H)-homohopane (22S)

C$_{31}$HR = C$_{31}$ 17α(H),21β(H)-homohopane (22R)

C_{32} S/(S+R) = C_{32} 17α(H),21β(H)-bishomohopane (22S)/C_{32} 17α(H),21β(H)-bishomopane (22S + 22R)

C_{35}(S+R)/C_{31}(S+R) = C_{35} 17α(H),21β(H)-pentahomohopanes (22S + 22R)/ C_{31} 17α(H),21β(H)-homohopanes

(22S + 22R)

C_{35}/C_{34} (S only) = C_{35} 17α(H),21β(H)-pentahomohopane (22S)/ C_{34} 17α(H),21β(H)-tetrahomohopane (22S)

C35 Homohopane Index = C_{35} 17α(H),21β(H)-pentahomohopanes (22S & 22R)/$\sum C_{31}$– C_{35} 17α(H),21β(H)-

homohopanes (22S & 22R)

Tricyclic Terpanes = sum of C_{19} to C_{30} tricycic terpanes

Pentacyclic Terpanes = sum of Ts, Tm, C_{28}BNH, C_{29}H, C_{29}Ts, C_{30}DiaH, Normor, C_{30}H, C_{30}Ts, Mor, Gam &

C_{31}– C_{35} 17α(H),21β(H)-homohopanes (22S & 22R)

Steranes (*m/z* 217 & 218)

C_{27} ααα 20R = C_{27} 5α(H),14α(H),17α(H)-sterane (20R)

C_{28} ααα 20R = C_{28} 5α(H),14α(H),17α(H)-sterane (20R)

C_{29} ααα 20R = C_{29} 5α(H),14α(H),17α(H)-sterane (20R)

C_{27} Dia/(Dia+Reg) = C_{27} 13α(H),17α(H) diasteranes (20R + 20S)/(C_{27} 13α(H),17α(H) diasteranes (20R + 20S)

+ C_{27} 5α(H) steranes (20R + 20S))

C_{29} αββ/(ααα + αββ) = C_{29} 5α(H),14β(H),17β(H)-steranes (20R + 20S)/

(C_{29} 5α(H),14α(H),17α(H)-steranes (20R + 20S) + C_{29} 5α(H),14β(H),17β(H)-steranes (20R + 20S))

C_{27} αββ 20(R+S) = C_{27} 5α(H),14β(H),17β(H)-steranes (20R + 20S)

C_{28} αββ 20(R+S) = C_{28} 5α(H),14β(H),17β(H)-steranes (20R + 20S)

C_{29} αββ 20(R+S) = C_{29} 5α(H),14β(H),17β(H)-steranes (20R + 20S)

C_{29}/C_{27} αββ Sterane Ratio = C_{29} 5α(H),14β(H),17β(H)-steranes (20R + 20S)/ C_{27} 5α(H),14β(H),17β(H)-

steranes (20R + 20S)

Triaromatic Steroids (*m/z* 231)

C_{26} Triaromatic Steroids = C_{26} Triaromatic Steroids (20R + 20S)

C_{27} Triaromatic Steroids = C_{27} Triaromatic Steroids (20R + 20S)

C_{28} Triaromatic Steroids = C_{28} Triaromatic Steroids (20R + 20S)

C_{29} Triaromatic Steroids = C_{29} Triaromatic Steroids (20R + 9α20S + 9β20S)

C_{20} = C_{20} Triaromatic Steroid

C_{21} = C_{21} Triaromatic Steroid

C_{26} 20R = C_{26} Triaromatic Steroid 20R

C_{26} 20S = C_{26} Triaromatic Steroid 20S

C_{27} 20R = C_{27} Triaromatic Steroid 20R

C_{27} 20S = C_{27} Triaromatic Steroid 20S

C_{28} 20R = C_{28} Triaromatic Steroid 20R

C_{28} 20S = C_{28} Triaromatic Steroid 20S

C_{29} 20R = C_{29} Triaromatic Steroid 20R

C_{29} 20S9α = C_{29} Triaromatic Steroid 9α,20S

C_{29} 20S9β = C_{29} Triaromatic Steroid 9β,20S

Polycyclic Aromatic Hydrocarbons & Benzothiophenes (*m/z* 178, 184, 198, 226 & 252)

BaP = Benzo(a)pyrene

BbF = Benzo(b)fluoranthene

P = Phenanthrene

MP = Methylphenanthrenes

C2P = Ethyl & dimethylphenanthrenes

DBT = Dibenzothiophene

MDBT = Methyldibenzothiophenes

C3DBT = Propyl, methyl-ethyl & trimethyldibenzothiophenes

Aromatic Maturity Indices (*m/z* 178, 192)

MPI-1 = methylphenanthrene index = 1.5[2-MP + 3-MP]/[P + 1-MP + 9-MP]

MPR = methylphenanthrene ratio = 2-MP/1-MP

Rc (%) = calculated vitrinite reflectance = 0.6(MPI-1) + 0.4 (Radke and Welte, 1983)